Review Paper:

A Review on Synthesis, Characterization and Photocatalytic Applications of Copper Oxide Nanostructures

Alebachew Nigussie, Ananda Murthy H.C.* and Abdissa Bedassa
Department of Applied Chemistry, School of Applied Natural Science, Adama Science and Technology University, P O Box 1888, Adama, ETHIOPIA
*anandkps350@gmail.com

Abstract

This review intends to give an overview of synthesis and characterization of copper oxide nanoparticles (CuO NPs) for photocatalytic applications. Cupric oxide (CuO), with a narrow band gap of 1.2 eV, is currently being applied in many fields such as photocatalytic, antimicrobial, energy conversion and optoelectronic devices applications because of its versatile functionalities and low cost. In addition, various nanostructures of CuO such as nanoparticles, nanocrystals, nanorods, nanocubes, nanosheets have found applications in catalysis, solar cells, batteries and gas sensors.

In this review, electrochemical, green, facile chemical solution, planetary ball mills precipitation, wet chemical and other synthesis methods are highlighted. In addition, the review also presents the detailed discussion on characterization of CuO NPs by techniques such as UV–visible, XRD, FT-IR, TEM, SEM, FESEM, TGA-DSC, DLS and AFM for exploring their morphology, crystallinity, size and shape. Current studies of drastic improvement in the dye degradation due to size and shape of the CuO nanostructures are also discussed. Generally, this review covers properties, synthetic methods and recent research progress of CuO NPs and their applications towards environmental remediation.

Keywords: CuO Nanoparticles, Photocatalysis, Dye degradation, Environmental remediation.

Introduction

Nanotechnology gained much attention for its vital pioneering role in manipulating materials at the atomic and molecular levels to dramatically alter the product properties. Materials reduced to the nano metric scale display significantly different properties compared to what they display at the macroscale or microscales. Because of their unique properties, nanomaterials are widely used in various applications. Nanostructured oxide powders are innovative materials obtained by new synthetic processes.

According to literature, the increasing use of NPs in medicine has led to a growing number of studies exploring potential antibacterial mechanisms of metal NPs which can change the metabolic activity of bacteria. This capacity represents a huge advantage in terms of eliminating bacteria to cure diseases.[1-2]

Semiconductors nanoparticles are becoming more and more important day to day as they play a tremendous role in a wide variety of scientific fields. Because of their novel properties like enhanced light absorption, quantum confinement, high specific surface area etc., semiconductor nanoparticles have huge contribution in solving global water and air purification, photocatalytic disinfection, medicinal and environmental problems and create tremendous opportunities in extending their applications. However, photocatalytic and antimicrobial activity of these materials are still far from that required by commercial applications and therefore in this area further studies are highly crucial.

In recent years, the research on CuO NPs for various applications has attracted worldwide attention. The study of CuO NPs conducted earlier[3] created great contribution for their future outlook of semiconductor photocatalysis semiconductors. In this study, new semiconductor-based nanostructured materials are recommended that would use lower-energy photons available in the visible spectral region. Addition of noble metal nanoparticles to TiO_2 was used for some time to enhance its photocatalytic activity as they can scavenge photogenerated electrons and thus increase electron−hole pair separation.

The prospect of potential applications of CuO nanostructures has led to substantial research and development efforts to have various types of nanostructures.[4] Similar studies on CuO show that CuO is a p-type semiconductor with a band gap of 1.2 eV and large surface area whose reactive morphology is particularly fascinating. This is due to its good chemical and thermal stability, low cost, low toxicity, ease of handling and high catalytic reusability.[5] CuO nanoparticles are stable, robust and have longer shelf life compared to organic and microbial agents.[6] Nanosized materials CuO NPs are prepared via several methods like sonochemical,[7] direct thermal decompositions, electrochemical methods,[8] colloid thermal synthesis process,[9] and green method etc.

Apart from interfacial interactions, morphology and size dependent properties are an important characteristic that influence the performance of CuO NPs for target application. Hence, in the attempt to develop CuO NPs, a long-standing objective is to develop facile strategies to

control the morphology, size, shape and composition. This control allows the tuning of chemical and physical properties CuO NPs.

In medicinal applications, CuO NPs have potential for external uses as antibacterial agents in surface coatings on various substrates to prevent microorganisms from attaching, colonizing, spreading and forming biofilms. Many researchers recommend mechanisms of antimicrobial response of CuO NPs in different species of bacteria which should be further investigated. Moreover, comparing and knowing the current status of the research area of CuO NPs will provide huge information and give various opportunities for investigation of new innovative approaches.

The aim of this review paper is to summarize the currently undergoing synthesis and characterization techniques of CuO NPs for photocatalytic and antimicrobial applications. In this regard, the review highlights various studies on photocatalytic and antibacterial activity tests of CuO synthesised from different precursors. It also tries to cover properties, synthesis methods and recent research progress of CuO NPs and its applications in the field of medical and environmental remediation.

Synthesis and structural characterization of CuO nanoparticles: Many preparation methods are reported to synthesize CuO NPs for different applications. This material can be produced by using various techniques typically classified as bottom-up (chemical methods) and top-down (physical methods). Bottom-up mainly involves wet chemical synthesis methods in which nucleation and growth of liquid substance take place. This technique has advantage of uniform size and shape of particles with fewer chances of surface defects and impurities. In addition, materials prepared by this approach are almost at the thermodynamically equilibrium state.[10]

Synthetic methods: The shape and size of the CuO nanocrystals are influenced by the reaction of Cu $(NO_3)_2$, oxalic acid (OA) to form Cu–oxalate. Synthesising of CuO NPs with different shapes and sizes by thermal decomposition of Cu–oxalate has been done by controlling the Cu: OA molar ratio and the CuO/TiO_2 core/shell structure using the hydrolysis of titanium isopropoxide (TIP) on the surface of monoclinic CuO nanocrystals. This influences photo catalytic properties of the obtained CuO nanocrystals. The systematic study of XRD pattern confirmed the presence of monoclinic CuO and the consistent size of particles with the corresponding SEM images of various shapes dependent on temperature, reaction time and ratio of Cu-Oxalic acid.[11]

Similarly, controlling size and morphology over the characteristics of nanoparticles by varying the temperature and the duration of the decomposition process, the multifunctional CuO nanosheets[12] were synthesized by thermal decomposition of $Cu_4(SO_4)$ $(OH)_6^-$ porous clay heterostructures (PCH) approach. The results revealed that PCH acts as a host material for spherical CuO NPs with particles size less than 10 nm.

A study[13] shows the advantage of electrochemical (EC) method as a cost effective and resourceful method of preparation under different reaction conditions as in table 2. TEM images confirm a good agreement between particle size and crystal size indicating the highly crystalline nature of the particles. Among different electrolytes at various calcination temperatures of 300 and 900 ^{o} C, round shaped particles with average particle size 20 and 25 nm at 900 ^{o} C were obtained in sodium hydroxide and sodium carbonate respectively. The observation of effect of electrolysis time on size and morphology of CuO NPs at 30, 60 and 120 min shows that whenever the electrolysis time increases, yield of product and size of particle also increased.

Irrespective of the preparation method used to obtain ultrafine CuO NPs, some researchers take the advantage of simple precipitation technique.[14-16] In this respect, Zhang et al[14] observed the effect of organic ligands on the shape of CuO nanostructures. First, the black CuO material is dried in a vacuum oven at 50 ^{o}C overnight and is calcined in air at 400 ^{o}C for 1.5 hrs. This procedure is repeated with the addition of 15 mmol of trisodium citrate dehydrate, sodium tartrate and sodium acetate trihydrate into three separate sets of copper solutions (0.05 M) to obtain leaf shaped CuO.

According to these authors, due to the differences in the coordination ability, steric effect and interaction with copper ion, the effectiveness of the CuO nanostructures as catalysts for the Rochow reaction are not same. Various shapes of CuO catalysts, FESEM images (Figure 10 a) leaf, urchin, flower and oatmeal-shaped and different exposed surfaces are prepared using different chelating ligands (acetic, citric and tartaric melt). The authors apply different morphology and shape (leaf, urchin, flower and oatmeal-shaped) of black CuO NPs on to those different organic ligands.

Likewise, a set of CuO NPs of different sizes and shapes are tested in XPS system for the Cu, O and C from the precursor. The XPS study identified the presence of Cu, O and C (Figure. 7 c and d) in all the four crystals. The peaks at 943.8 and 962.8 eV revealed the formation of pure CuO crystals. In addition, the appearance of three distinct and narrow peaks at 663, 574 and 458 cm^{-1} in FTIR spectra for all the CuO nanostructures further revealed the formation of high-quality monoclinic CuO (Figure 1).

The development of synthesis of nanomaterials over a range of sizes, shapes and chemical composition is an important aspect of nano technology. The precipitation method when stabilized by *in situ* capping agent, triphenylphosphine oxide (TPPO) can produce highly stable CuO NPs with optical band gap of 2.29 eV.[15] A few precipitation techniques were also employed[16] and also used to synthesize crystalline nature of CuO NPs for antimicrobial application. Structural

study by Field emission scanning electron microscope (FESEM) and Field emission transmission electron microscope (FETEM) revealed the morphology of CuO NPs. TEM and XRD study analysis determined the average diameter to be 23 nm.

In the study of the effect of solvents, a remarkable hydrolysis method[17] was reported to synthesize CuO nanostructures to test for photocatalytic activity. CuO nanostructures of different morphologies, nano dots and nano aggregate are prepared from different solvents and resynthesized via mild alterations. SEM study reveals nano dots and nano aggregate ranging from 5 to 1000 nm. A linear correlation was found between the band gap energy and average size of the single constituent NPs, which shows a confirmation to their size estimations made through the Scherrer's equation.

Various wet chemical techniques such as, sol-gel, co-precipitation, combustion etc., are applied to synthesise wide range of multicomponent nano crystalline oxide powders. A sol–gel process which is a popular approach for the preparation of metal oxide structures,[17] showed fabrication of CuO nanoflake for antibacterial application. Structural analyses by XRD revealed the monoclinic structure of CuO NPs. Study of morphology and elemental composition by SEM and EDS exhibited nanoflake like structure. Corresponding FT-IR study confirmed the presence of three different bands correspond to the Cu-O bond vibrations. Similarly, a simple wet chemical method continuously synthesised inorganic nanoparticles with particle sizes smaller than 100 nm in very short mixing times.

CuO NPs and nanolayers by sol–gel and spray pyrolysis methods were also reported.[19,20] XRD pattern of the CuO nano layer reveals that the sample has a crystalline structure, uniform distribution of particle size and a homogeneous morphology. Three different bands which correspond to the Au and Bu modes were found on the nano layer of CuO NPs through TEM and SEM images.

Similarly, the wet chemical method[21] was employed to synthesise CuO nanosheets to study the impact of polyvinyl pyrrolidine (PVP) on the morphological and photocatalytic behavior of CuO nanosheets. Copper nitrate trihydrate ($Cu(NO_3)_2 \cdot 3H_2O$) and sodium hydroxide (NaOH) with various amount of PVP (0, 0.1 and 0.2 g) were used as starting materials. Characterization studies confirmed the formation of nanosheets like structures with average widths of the samples P1, P2 and P3 58, 51 and 50 nm and the average lengths of 289, 268 and 264 nm respectively (Figure 2).

Besides the above highlighted methods, other researchres[22,23] have also synthesised flower-shaped hierarchical CuO microspheres by a facile refluxing. Information obtained from XRD confirmed formation of single phase CuO showing monoclinic crystal structure. Hierarchical flower-shaped CuO microspheres are observed by SEM. UV–vis spectroscopy revealed absorption between 700 and 950 nm and the calculated band gap to be 1.59 eV.

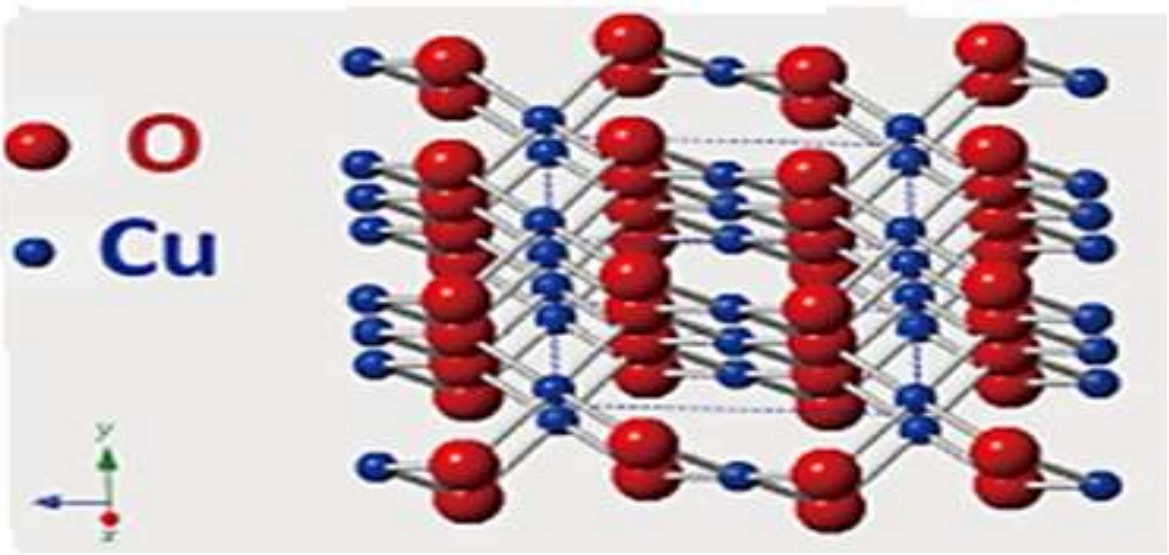

Fig. 1: The crystal structure of CuO[14]

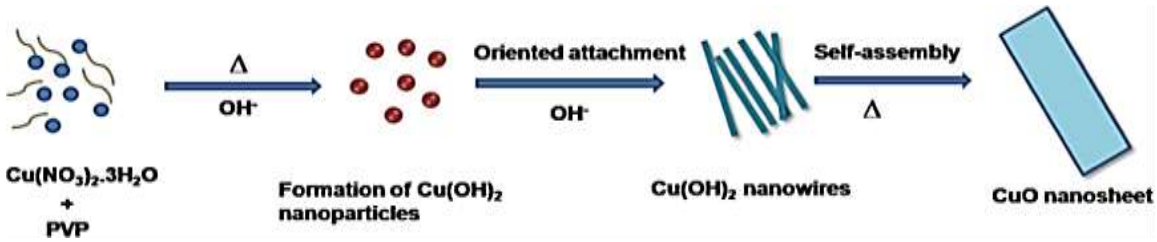

Fig. 2: Schematic of growth mechanism of CuO nanosheets[21]

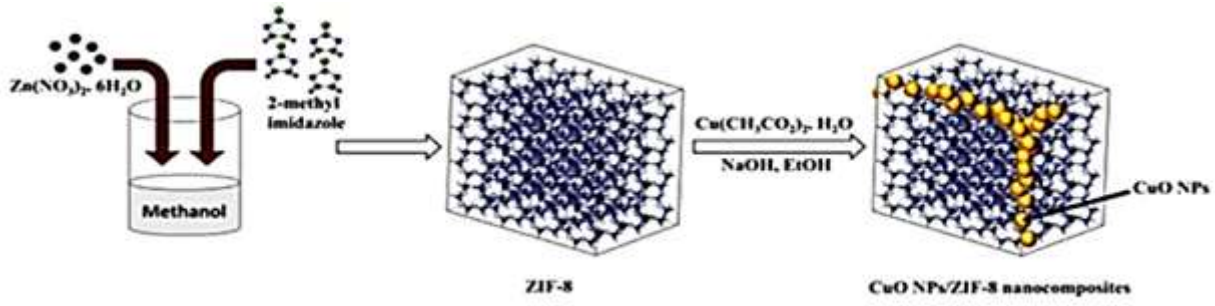

Fig. 3: Schematic representation for the formation of CuO NPs/ZIF-8 nanocomposites[33]

As presented above, several approaches have been employed to enhance the applications of CuO NPs including surface modification, band gap engineering with various shapes and sizes. An inexpensive and simple quick simple solution process was also proposed.[24] CuO nano cocoons (spindle-like morphologies in which the central part is wide while the corners are narrow) were synthesised at low temperature. Researchers took advantage of solution combustion method to synthesize CuO of various morphologies and applications.[5,24,27]

With some modifications of methodology described above, CuO nanoflowers[25] with band gap of 3 eV were prepared for the photocatalytic application. CuO sheet-like nanostructures were fabricated[26] with band gap energy about 2.31 eV by a facile solution phase chemical method from ethanol and water mixture solvents for photocatalytic activity. This smaller band gap energy shows that CuO sheet-like nanostructures exhibit a strong quantum size confinement effect due to the shape of CuO NPs. Similarly, using solution phase method, CuO with even smaller band gap energy of 1.31eV was synthesised.[29]

The role of polyethylene glycol (PEG) molecules also regulates the surface energy of particles, avoids agglomeration and consequently reduction of particles size. FT-IR analysis of CuO NPs has three characteristic bands observed at 407 cm^{-1}, 490 cm^{-1} and 608 cm^{-1} indicating the existence of A_u and B_u modes of CuO. The UV–vis diffuse reflectance spectral investigation of the absorption of the maximum portion of the visible light shows the first notation that CuO used as the visible light responsive nano catalysis.

The plant extracts obtained from various leaves of plants *Azadirachta indica*, *Hibiscus rosa-sinensis*, *Murraya koenigii*, *Moringa oleifera* and *Tamarindus indica* have been compared with CuO NPs synthesised by chemical methods. The leaves of plants' extract are rich in phenols and flavonoids and were used as a reducing and capping agent. The effect of these reducing agents analyzed by FT-IR spectra of bands at 490 and 530 cm^{-1} assigned to metal-oxygen (Cu-O) vibration supports the presence of monoclinic phase of CuO NPs on XRD pattern.

The band at 1663 and 1674 cm^{-1} is due to amide whereas that at 1530 and 1535 cm^{-1} corresponds to the amide characteristic of proteins/ enzymes.[30] These demonstrate that due to lack of luminescence data, the low emission efficiency of CuO NPs and the origin of luminescence CuO remain contradictory but many emission bands between 420 and 650 nm were observed along with relatively high intensity peak at 735–740 nm.

The emission of several sub peaks from the new sublevel is due to band edge emission which might arise by the interaction of the two excitons or the 3D-1D splitting in Cu^+ ($3d^9$ $4s^2$).[31] However, theoretical calculations indicate that although Cu vacancies are most stable in CuO, they do not make any change in the electronic structures of CuO. Otherwise, oxygen vacancies or O_{Cu} antisite defects are responsible for these emissions while their formation energy is not much different from the formation energy of Cu vacancies.[32]

Recently, Imidazolate Frameworks (ZIFs), the sub-family of metal-organic frameworks (MOFs), have attracted increasing attention for different applications. A new approach of integrating the cubic shaped wide band gap (E_g = 4.9 eV) ZIF-8 prepared by sol-gel synthetic approach with narrow band gap CuO NPs was successfully produced.[33] A series characterization with TEM shows average size of the pristine ZIF-8 of 80–90nm. These uniform sized particles are deposited with CuO by reacting Cu $(CH_3COO)_2 \cdot H_2O$ immobilized ZIF-8 with NaOH in ethanol. Ultra-small colloidal CuO NPs with 5nm size are deposited and aggregated on the surface of cubic ZIF-8.

Figure 4b shows a high resolution TEM image of the CuO NPs/ZIF-8 nanocomposites where CuO NPs show a lattice spacing of 0.25 nm. FT-IR spectra of as synthesized ZIF-8 and CuO NPs deposited ZIF-8 photocatalyst with an absorption range of 400–2000 cm^{-1}. FT-IR spectrum of pure ZIF-8 and CuO NPs/ZIF-8 nanocomposites were used to observe new absorption bands appearing in the nanocomposites. The absorption in between the region of 424–680 cm^{-1} belongs to the CuO nanoparticles.

Particularly, the appearance of a band at 530 cm^{-1} is assigned to the characteristic stretching vibration of Cu-O of monoclinic nanoparticles.[34] The band gap value of pristine ZIF-8 assessed from the steep absorption edge is ~5.38 eV. Whereas, the band gap decreases by 0.45 eV (Eg = 4.93 eV)

in CuO NPs deposited ZIF-8 nanocomposites. On the other hand, the optical band gap of the isolated CuO NPs is estimated from the absorption onset (Eg = 2.05 eV) and showing a good agreement with the reported value (Eg = 2.1 eV) for CuO nanoparticles of 5–10 nm. The photoluminescence (PL) properties of pure ZIF-8 and CuO NPs/ZIF-8 nanocomposites examined the PL spectra of nanocomposites material upon excitation at 350 nm.

The PL spectrum for the CuO NPs/ZIF-8 nanocomposites exhibited the double emission bands in the visible region. The emission band at 424 nm (blue) originated due to the recombination between electron in the conduction band and the holes in the valence band. The long wavelength emission at 483nm (blue) is originated due to deep level emission such as oxygen vacancies and Cu-interstitials. Besides this result, the thermogravimetric analysis (TGA) of as-synthesized ZIF-8 and CuO NPs deposited ZIF-8 under nitrogen atmosphere. The weight change profile of neat ZIF-8 reveals a very weak 2.5-wt% weight loss before 180 ^{o}C and corresponds to the removal of solvent or other guest molecules (methanol) blocked within the ZIF-8 framework.

The weight loss exhibited in the temperature range of 180–500 ^{o}C, is associated to the decomposition of some adsorbed 2-methyl imidazole linkers. The third weight loss occurs from 500 ^{o}C and is attributed to the decomposition of framework structure. The ZIF-8 structure is stable up to 500 ^{o}C.[35] However, the TGA curve (Figure 6b) of CuO NPs/ZIF-8 nanocomposites indicates the increase in stability of the compound up to 600 ^{o}C compared to ZIF-8.

The study shows the 2% weight loss occurred from 90 to 150 ^{o}C which is attributed to the loss of some loosely bound solvent molecules present in the framework structure. The second step weight loss occurred in the temperature range of 150–600 ^{o}C and is due to decomposition of some adsorbed organic linkers. The last weight loss which occurred from 600 ^{o}C, is associated to the decomposition of framework structure of nanocomposites.

Because of their wide usage in various applications such as manufacturing antibacterial materials, solar cells, gas sensors, photovoltaic cells, as well as drag reduction and catalysis, there is a great interest to synthesize CuO NPs from different substrates and by different methods as depicted in table 1. Specific properties of materials on the nanoscale have a large brunt on catalysis, antimicrobials and biosensors that led to the evolution of new technologies.

Focusing on the recent activity of colloidal gas aprons (CGA) or gas aprons which are surfactant stabilized micrometer size gas microbubbles are used as substrate for the mass production of CuO NPs. This procedure is a simple and cost-effective method. The corresponding FESEM study helped to have the nanoscale (below 100 nm) and high–resolution transmission electron microscopy (HRTEM) shows the shape and average diameter15–30 nm CuO NPs.

Thermal gravimetric analysis (TGA) elucidate the shell nature of the synthesis temperature to be at 300 ^{o}C, hence at this temperature, all absorbed water evaporates without damaging the anionic surfactant, sodium dodecyl sulfate (SDS) structure which was used to examine the presence of C-H groups by FTIR and also minimized particle agglomeration.[36]

Conducting on the photo degradation behavior of CuO NPs with different shape and size can improve its efficiency. But its elemental composition depends on the substrate used and the method of synthesis technique.

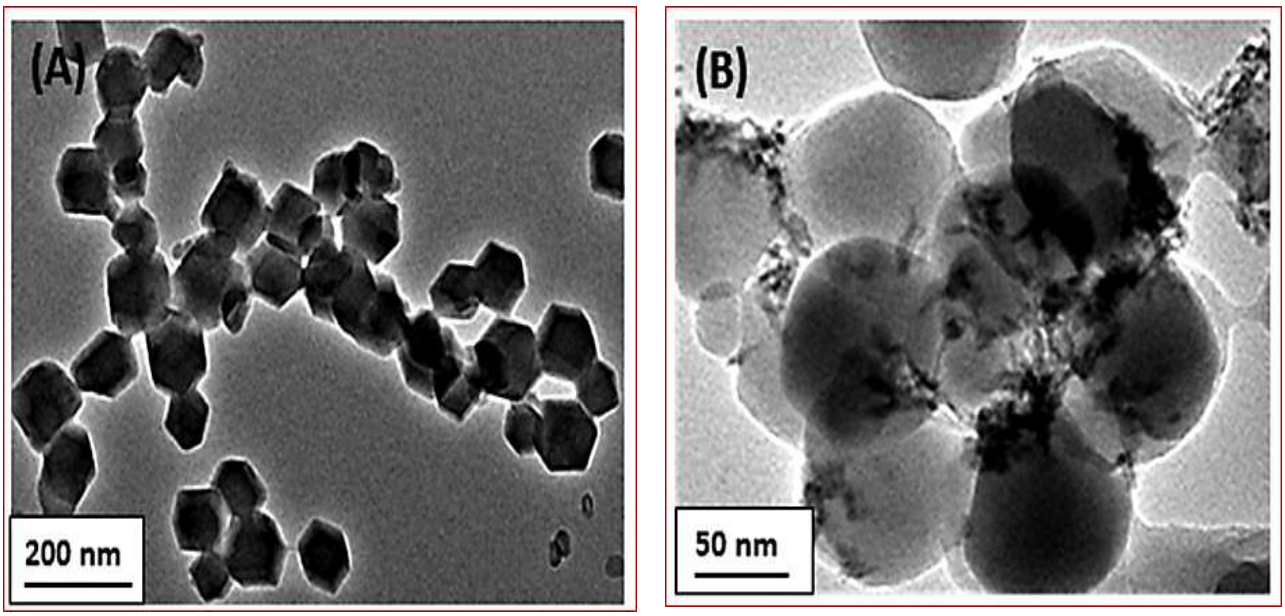

Fig. 4: (a) Representative TEM image of ZIF-8 at low magnification (b) TEM images of 5-wt% CuO NPs/ZIF-8 nanocomposites at high magnification[33]

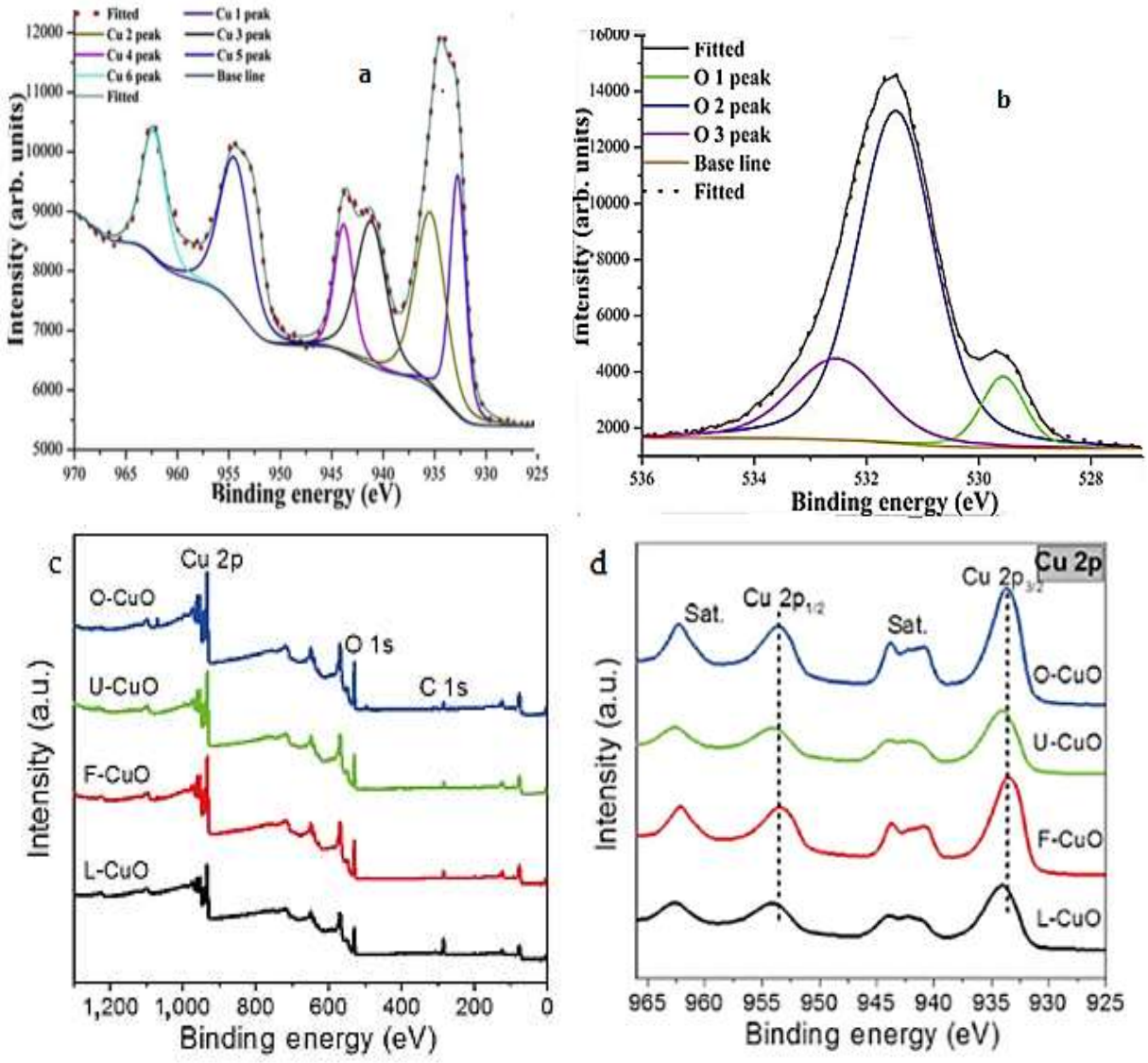

Fig. 5: XPS spectra of the CuO catalysts synthesised from various sources[14,37]

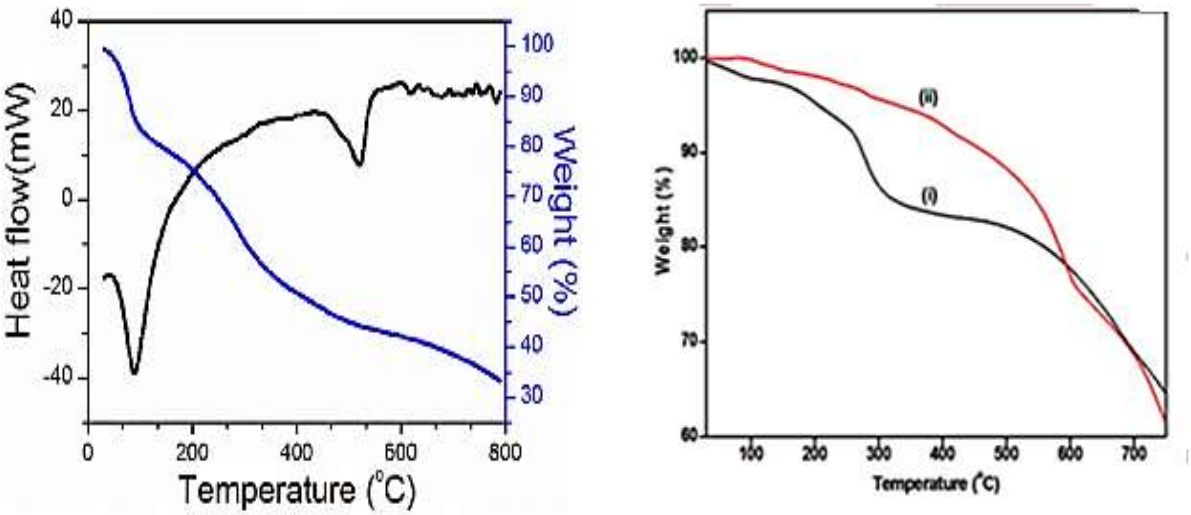

a. TG-DSC of CuO nanoparticles[38]

b. TGA curves of (i) ZIF-8 and (ii) 5-wt% CuO NPs/ZIF-8 nanocomposites[33]

Fig. 6: TGA-DSC of CuO NPs

For instance, CuO nano leaves[39] were synthesised (NLs) with band gap energy of 2.15 eV having different sizes from aqueous solution of $CuSO_4$.$5H_2O$, L-arginine and NaOH under vigorous stirring microwave method. Investigation of size distribution and morphology of the prepared CuO nanoparticles by TEM and HRTEM images confirm the formation of 2-dimensional leaf-like morphology.

The effect of surfactant cetyl trimethylammonium bromide (CTAB) on degree of aggregation controls the grain size and shape of nanostructures as well as morphology of CuO nanosheets.[40] Figure 9d and e show low magnification SEM and high magnification image of CuO nanostructures respectively. The latter figure is a hierarchical CuO nanosheet of different sizes composed of aggregating nanorods of different lengths and widths. The nanosheets CuO NPs show very sharp edges having a smooth surface of active crystal facets absorbing more light. The collected PL spectrum is indicated at excitation wavelength 45 nm. Due to the quantum effect arising from reduced particle size, the blue shift in the band gap of CuO nanostructures is observed in the calculated band gap of 1.34 eV.

Several insightful reviews which are benchmark on enviromental and medicinal applications develop an impressive insights on CuONPs. The fundamental overview of antimicrobial properties of various photocatalyst metal oxides including CuO NPs and the potential applications as surface coatings have been discussed by few researchers.[41] The other group[42] developed the effect of some general factors on the morphology and properties of CuO nanomaterials prepared by solution methods. Most of these reviews[43] focus on either synthesisng and characterization of CuO NPs or only or general applications of CuO NPs. But currently many studies focussed on synthesisng and photocatalytic and antimicrobial application of CuO nanomaterial. From these studies we perceive significant role of parameters and reagents on size, shape and morpholgy of nanomaterials.

Fig. 7: Schematic illustration of formation of CuO nano leaves[45]

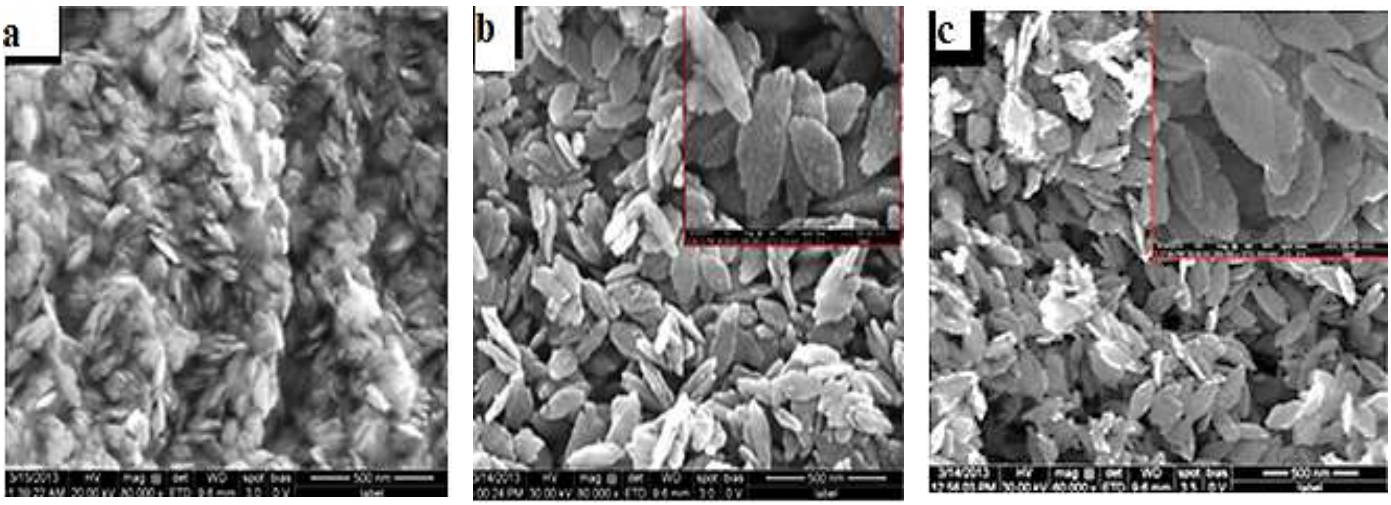

Fig. 8: FESEM images of CuO nanoleaves: (a) without sodium citrate, (b) with 0.05 M sodium citrate, (c) with 0.1 M sodium citrate[45]

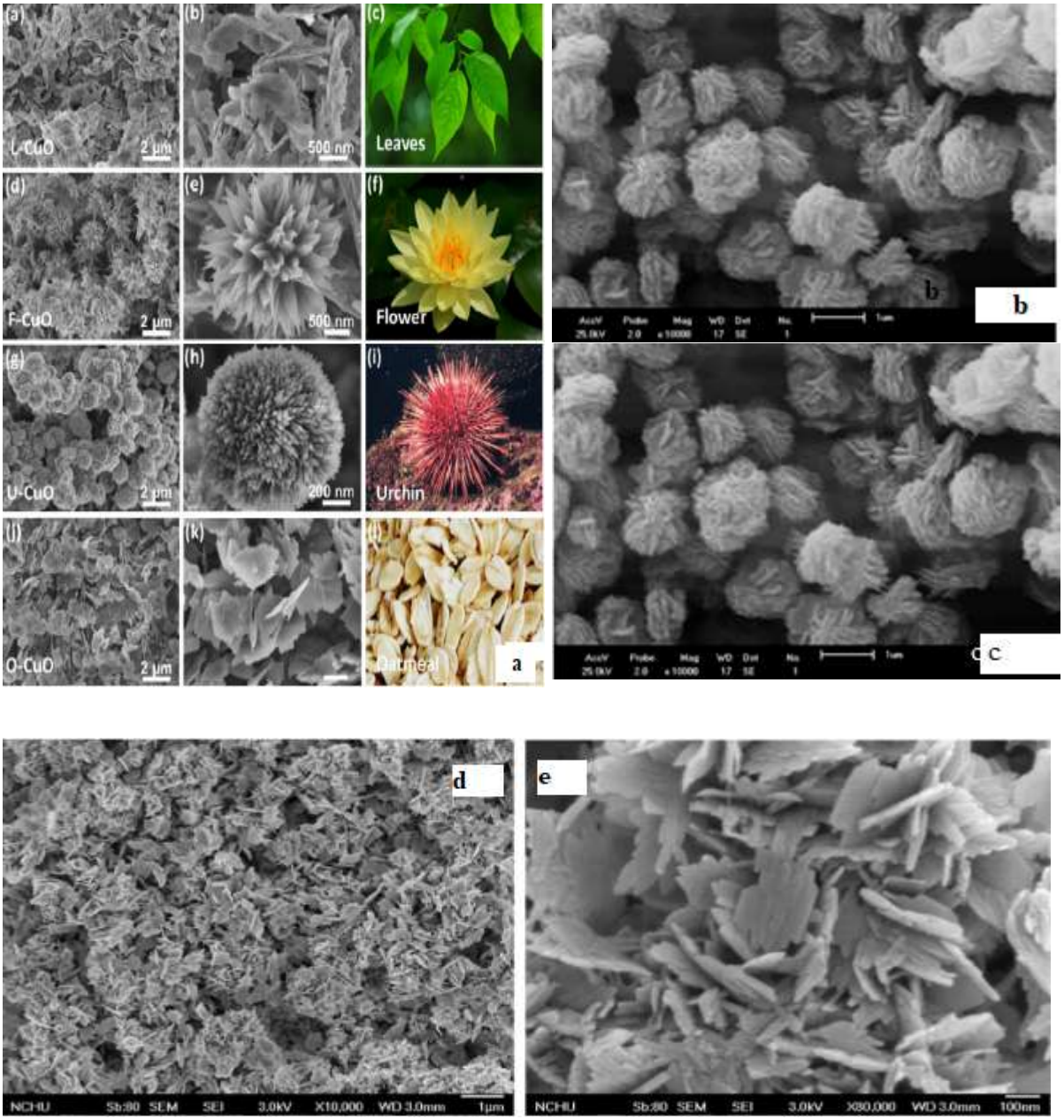

Fig. 9: Representative SEM images of different shapes of CuO NPs[40,44]

CuO NPs[44] were prepared by using two different alkaline oxides (NaOH) and (NH_4OH) at pH=13 and 10 from precursor Cu (NO_3)$_2$ $3H_2O$ by microwave hydrothermal method under mild conditions of low temperature and short time. Due to the basic strength of alkalis, the fabricated material led to different pH of different morphologies. The CuO monoclinic nanostructures with single phase have been identified by XRD and SEM. FT-IR spectra of both samples have shown vibrational modes at 506 cm^{-1}, high frequency mode at 570 cm^{-1} and 603 cm^{-1}. SEM images for both samples, NH_4OH and NaOH (Figure 9 b and c) respectively represent plate-like particles morphology.

The sample prepared from NH_4OH shows mass of seemingly spherical shape where as CuO NPs prepared from NaOH result in the interconnected channels. According to the authors, this is because the previous material has some smaller quasi-spherical agglomerates while others are larger than a micrometer resulting in a small particle size, but the difference between the two samples is in the agglomeration. Highly stable CuO nanpleaves[45] were prepared with average sizes of 250–300 nm by using hydrothermal method with band gap energy ranging from 2.67 to 2.97 eV. The morphology of the CuO prepared with and without sodium citrate was observed via FESEM.

Figure 8 a, b. and c show aggregated seed-like CuO nanostructures of length 50–100 nm without citrate whereas leaf-like CuO nanostructures were with length of 150–200 nm using different concentration of sodium citrate. On increasing the concentration of citrate to 0.1 M, CuO nanoleaves with a width 50–100 nm and length of 250–300 nm were produced. This is due to capping agents modulating

the kinetic growth and determining the subsequent morphologies of the final products.

A three-step synthesis of CuO particles was reported[46] which displayed spindly shapes with crystal faces of monoclinic sustem. Structural studies revealed image of a single particle showing a shape similar to carambola composed of nanosheets with a thickness of a carambola. It had ~1 μm length and 300 nm width. The authors proposed three typical schemes for the formation of CuO:

a. Production of Cu $(OH)_2$ clusters,
b. HMTA-controlled growth of Cu $(OH)_2$ nanosheets around the clusters and
c. Decomposition of Cu $(OH)_2$ to CuO.

To synthesize metallic oxide capable of withstanding high temperature and pressure, high energy ball milling is a robust and energy efficient synthesis method. It generates NPs with various shapes and dimensionalities. In high energy ball milling process, the moving balls transfer their kinetic energy to the milled material. This results in the breaking of their chemical bonds and rupturing of the milled materials into smaller particles with newly created surfaces.[47] CuO spherical-like NPs by the planetary ball mill method were fabricated.[48] The effect of different milling times investigation shows that the smallest particle size of 82nm is achieved by ball milling at dry medium during 20hr.

The preparation of metal oxide nanocrystals with controlled nanocrystal size, composition and internal structure has a great contribution for further nano technology advancement. For instance, CuO was synthesised by solvothermal route with subsequent calcination and fabricated hexapod nanostructures with average diameter of 1.2 μm, monoclinic phase and porous structure. Nitrogen adsorption–desorption isotherm as well as the pore size distribution revealed the porous structure of the as-prepared CuO nanocrystals.

A simple, environmental safety and fast top down procedure[50] to prepare CuO nanowires by a thermal process in oxygen ambient of a Cu foil is another alternative approach. Structural characterization by SEM confirms formation of nanowires (NWs). Chemical composition investigation by XRD and EDX analysis reveals the presence of mixture of both CuO and Cu_2O. Thermal evaporation combined with aging in oxidizing ambient has great impact on morphological, optical and structural behavior of CuO thin film and photocatalytic activity.

The effect of thermal annealing in the morphological, optical, structural and photocatalytic behavior of CuO nanostructured thin film can be studied by advanced structural characterizing techniques.[51] For example, figure 10 (a–d) shows the FESEM images of CuO thin films annealed at 400 ^oC and 600 ^oC. This clearly shows that annealing resulted in growth of CuO nanostructures in the CuO thin film.[52]

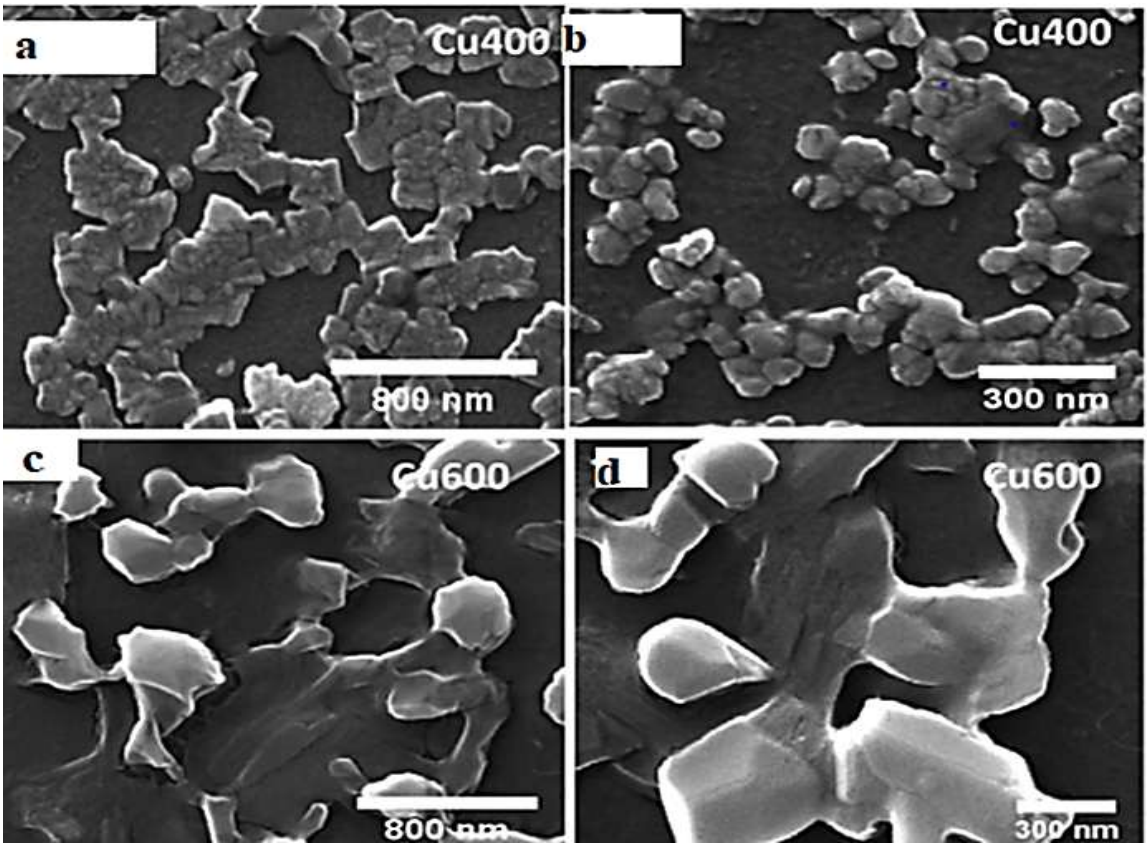

Fig. 10: FESEM images of the prepared CuO thin film samples annealed at 400 and 600 ^{o}C[51]

Carbonaceous particles with surface functional groups are used for metal ion adsorption, hence shells may be formed by supplying enough shell precursor material to the sacrifice carbonaceous spheres. CuO hollow microspheres[53] were fabricated successfully with different shell thickness and porosity using carbonaceous microspheres (CMS) as the sacrificial templates through the emulsion polymerization reaction of sucrose under hydrothermal conditions. In this work, various hollow spheres of CuO are synthesised by dispersing freshly-prepared CMSs (0.6 g) in 1 M, 2 M, or 3 M copper nitrate solution. Shell thickness and the porosity are influenced by the Cu^{2+} concentration and the ethanol content of the aqueous infusion solutions. Hence, the more concentrated the Cu^{2+} is in solution, the more Cu^{2+} can be adsorbed within the CMS templates.

Green method: Several physical and chemical methods used in the synthesis of CuO NPs raise several problems like high temperature and pressure, reducing agents, organic solvents and hazardous chemicals. To meet this technological need and mitigate the drawbacks, use of plants as a sustainable route for synthesis is proposed in many studies. The development and design of nanoparticles based on green chemistry principles which include nontoxic chemicals, renewable material, environmentally benign solvents and finally degradable waste product have significant roles for the green synthesis approach of nanoparticles.

The most common CuO nanofabrication methods like hydrothermal and solvothermal methods are known for manufacturing metal oxide nanostructure materials. Laser deposition, chemical vapor deposition (CVD), electrochemical methods and microwave or ultrasonic irradiation methods are also used exhaustively. However, these existing methods sometime create harmful impression such as contamination with impurities, use of strong acid or strong alkali solutions, high temperature and high-pressure requirements, or vacuum environments. Currently, many scholars apply an environmentally kindly fabrication process at normal temperature and normal pressure desired to obtain high-quality products via a low-cost method.

Submerged photo-synthesis of crystallites (SPSC) is a photo-synthetic method that can produce nanocrystals in neutral aqueous environments with UV or visible light. A study on the production of flower-like CuO[54] nanostructured surfaces via (SPSC), by irradiation with UV illumination in neutral water was reported. Structural studies by FE-SEM confirm images of the surface subjected to UV irradiation after SPSC with the plasma treatment (Figure 11). EDS show components of the nanoflowers to have a CuO composition.

An environmentally friendly combustion method[55] was used to synthesize CuO NPs from the extract *Abutilon indicum* for antimicrobial and antioxidant and photocatalytic activities. Even though synthesized nanoparticles are structurally not homogenous, XRD, EDX and SEM results confirmed successful synthesis of CuO NPs, with hexagonal, wurtzite and sponge crystal structure. Due to the energy band gap confinement effect, the band gap energy located as 3.378 eV is slightly higher than normal.

A biosynthesis approach[56] was reported in the fabrication of CuO NPs from alga extract for antimicrobial application. Shape and size of the resultant particles elucidated with TEM show spherical shape ranging from 5 to 45 nm respectively.

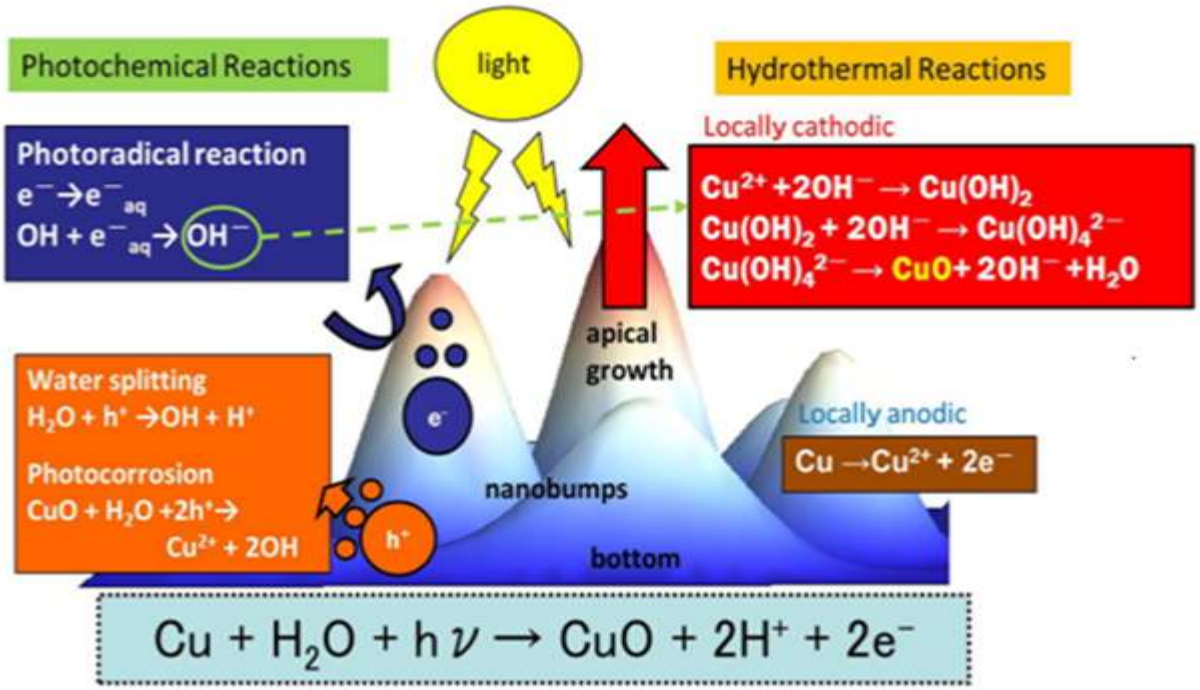

Fig. 11: A schematic view of the mechanism of CuO crystal growth in the SPSC process[54]

Inexpensive, simple and novel biosynthesis approaches were reported for the synthesis of Cu NPs from different types of plant resource extracts[37,38,57-60] as reducing, stabilizing, capping, chelating and protecting agents using neither hazardous chemicals nor high temperatures. Therefore, considering the functionality, low cost and non-toxicity, it is very important to optimize the reduction process and parameters. The preparation of CuO NPs from plant extracts results in various shape, size and morphology. This may be due the effect of isolating process, presence of type of functional groups, capping agents etc.

The summary depicted in table 1 shows that the choice of synthesis method determines the physicochemical characteristics of the CuO NPs such as the size, dispersity, type of intrinsic and/or extrinsic defects, morphology and crystal structure. Characterization studies by UV–Vis absorption spectroscopy, XRD, SEM-EDX and TEM analysis confirmed formation of CuO NPs. All the analyses revealed the average size of CuO NPs to be 48 ± 4 nm in size. The presence of functional groups and chemical composition of CuO NPs are also confirmed by FT-IR spectrum showing bands in average at 471 cm^{-1} corresponding to metal–oxygen (M–O).

Apart from the above studies, the preparation of CuO NPs from *Tinospora cordifolia*[5] water extract of different concentrations produced images of sponge like structure. They anticipated that when alkaloids, steroids, diterpenoids, lactones, aliphatics and glycosides are isolated form the leaves of the plant by extracting with suitable solvents and when such an extract is employed for the combustion synthesis of metal nitrates, due to the process of reduction, metal oxide NPs can be produced. By using the Scherrer's formula, the authors calculated average crystallite size to be 6.5, 6.4, 6.47 and 8.47 nm for the extract concentrations of 0.2, 0.3, 0.4 and 0.5 g respectively. They conclude that fuel has played profound role in controlling particle size. In addition, the band gap values of 4.48 and 3.33 eV which are greater than that of the bulk CuO, may be due to the size effect of the NPs.

Taking the advantage of green method, CuO NPs[38] were fabricated with size 20–45 nm range through the phytogenic reduction of $CuNO_3$ to CuO derived from *Aglaia elaeagnoidea* flower extract. FTIR observation confirms the presence of different functional groups like proteins, phenolic compounds which are responsible for the synthesis; prevent agglomeration and act as capping agent. The presence of free amino and carboxylic groups contributed for the stability of CuO NPs. Thermal stability of the nanomaterial was observed by thermogravimetric analysis and differential scanning calorimetry at a heating rate of 10 ^oC /min in air over a temperature range of 30–800 ^oC. Figure 6a shows 22 wt. % weight loss between 30 to 200 ^{o} C. This is due to water evaporation, hence nearly 40 wt. % weight loss at 200–800^oC corresponds to organic matter decomposition (Flower extract) of the sample.[61]

The TEM analysis of CuO[58] synthesized from *B. tomentosa* leaf extract showed the particle morphology as spherical and the nanoparticles are moderately clustered with average crystallite size of 22-40nm. A similar study was reported[59] on green synthesis of CuO NPs from *Juglans regia* leaf extract. Results revealed that CuO NPs with smallest particle size (λ_{max} of 225 nm) and maximum concentration (5.010% a.u.) are fabricated using optimum synthesizing parameters including 1 g, of copper salt. Amount of walnut leaf extract is 14mL. The optimum temperature of furnace is recorded at 490 ^oC. According to the authors, minimum size of CuO NPs is obtained at minimum λ_{max} and maximum concentration at maximum absorbance.

A comparative study of nanoparticles synthesised from same plant parts extracts is not common but CuO NPs[61] were also obtained from Andean blackberry fruit (ABF) and leaf (ABL) extracts to evaluate antimicrobial activity. In addition to XRD and FT-IR studies, UV-visible spectra confirmed formation of two peaks of maximum absorption at 240 nm and 510 nm in ABF extract in addition, at 240 nm and 360 nm peaks in ABL extract. The presence of flavonoids, ellagic acid and tannins in berry leaves illustrates the presence of ABF/ABL extract composition of CuO NPs. When this composition increases, the absorption peaks become stronger and the maximum absorption of CuO NPs shifted from 250 nm to 255 nm.

Dynamic Light Scattering (DLS) studies revealed the average particle size of CuO NPs to be 43.3 and 52.5 nm for ABF and ABL respectively. The authors concluded that the ABF extract is more efficient than the ABL due to the synthesis of smaller size CuO NPs. Transmission electron microscopy selected area electron diffraction (TEM-SAED) study revealed spherical morphology with a mean size of 45 and 53 nm respectively.

Previous study on Black beans (Phaseolus vulgaris family: Fabaceae) argued that the black beans have high amounts of anthocyanin, protein, vitamins A, B and C, calcium and polyphenols. Polyphenolic compounds are used to reduce diseases caused by reactive oxygen and nitrogen species. A green synthesised spherical CuO NPs,[62] from an aqueous black bean extract can be considered as a new and cheap alternative treatment among expensive and creating side effects like surgery, chemotherapy and radiotherapy methods used in cancer treatment. So, this method is taken as an urgent need for effective, inexpensive and non-toxic, treatments with minimal side effects that are acceptable by people designing anticancer nanoparticles.

FT-IR bands located at 1037.6, 595.8 and 539.9 cm^{-1} were assigned N–H stretching vibrations of aliphatic amines, C–Cl stretching of alkyl halides and C–Br stretching of alkyl halides respectively.

The strong band is located at 1037.6 cm^{-1} whereas peaks at 595.8 and 539.9 cm^{-1} attributed to vibrations of CuO using

XPS. Raman shift and bandwidth change with decreasing particle size showing Raman intensity are related to the grain size. The firm peak at 286 cm^{-1} and a weak peak at 336 cm^{-1} are assigned to CuO.[63] The high-resolution XPS spectra of the Cu 2p (Figure 4a) show strong fitting peaks at around 932.7 and 935.5 eV for Cu $2p_{3/2}$ and 952.5 and 954.5 eV for Cu $2p_{1/2}$. The high-resolution XPS spectra of O 1s (Figure 3b) show that the core-level spectrum is broad and consists of three peaks that can be assigned to the O^{2-} in CuO NPs. The main peak at the lower binding energy of 529.4 eV is attributed to Cu–O. Images obtained from TEM confirmed the spherical shape of CuO NPs while SEM images are spherical, hexagonal and uneven shapes.

A highly aggregated colloidal CuO NPs[64] was fabricated with size of 3–40 nm by laser ablation method. *Eichhornia crassipes* leaf extract[65] was applied to prepare CuO nanoparticles. A new result reported of 2D CuO nano leaves (NLs) using amino acid, namely glutamic acid used as a complexing/capping agent via microwave irradiation technique. CuO NLs showed a blue shift to 2.1 eV with a decrease in grain size. Characterization studies show that size and shape of NPs depend on the duration of the ablation process and laser energy. An investigation of thermal plasma technology had been to synthesize CuO NPs,[67] reported. TEM energy dispersive spectroscopy displays the ratio of copper to oxygen elements to be 54.18% to 45.26%. A synthesis from selected medicinal plant identified by two methods, one with the visual observation of color change pattern and another one with UV–Vis analysis was also published.[68]

In this study, CuO NPs synthesized from fruit extract showed a color change pattern from brown to green color at the time of synthesis. The UV–Vis analysis of plant extract has exhibited a broad peak near 536 nm which specifies the presence of ascorbic acid to be reduced after synthesis of nanoparticles by exhibiting a small peak at 541 nm and a small peak around 217 nm. After synthesis of nanoparticles, the peak around 217 nm was shifted to a sharp peak at 285 nm. This was a good result to check the synthesized NPs of CuO having properties specifically, spherical shape, size (ranging from 2 to 69 nm), non-agglomerated and poly-dispersed nature.

Optical properties of CuO NPs: The structural and optical properties of CuO NPs are intensively studied by many researchers. The UV-Vis, FT-IR, band gap energy and others properties result have drawn considerable interest in recent years due to their interactive properties such as large surface-to-volume ratio and distinctive electronic and optical properties as compared to bulk materials. Attempts have been made to prepare and observe optical properties of CuO NPs using different preparation methods such as solution phase method,[28] green synthesised method,[37] planetary ball mill method,[48] solvothermal method,[49] thermal process,[50] ultrafiltration surface contact method (UMSCM), hydrothermal method and grounding method.[69]

In determining of the optical properties of CuO NPs, we observe that in addition to the synthesized method, different parameters like calcination temperature, pH, solvent, organic ligands and the type of precursor used have great contribution for variation of absorption coefficient of CuO NPs as a function of photon energy. Because of this reason, most of the studies disseminate similar optical properties. The XRD result are directly related to variations in the morphology and average surface area which may be due to the use of different organic ligands.[69] XRD study also shows 2θ value of commercial CuO NPs nearly same as that of prepared with the other three methods.

Moreover, types of crystals belong to orthorhombic crystals but the peak intensity of commercial CuO is higher than that of CuO prepared with the other three methods; the peak intensity of CuO prepared with the UMSCM was lower and broader. The particle size of the CuO made with UMSCM is smaller than that made by hydrothermal and ground methods. The calculated sizes with Sheerer are 144nm, 50nm, 32nm and 14nm for commercial, grounding, hydrothermal and UMSCM respectively. A recent study[70] on optical absorption shows that the direct band gap compared to indirect band gap permits was used to determine the crystallinity of a material. The calculated direct band gap value was 3.85 eV, which is higher than the bulk band gap value 3.5 eV.

From the above discussion, we perceive that the optical absorption spectrum is used to study the optical properties of the synthesized CuO NPs for intended applications. From this the band gap and the type of electronic transitions can be determined. Previous study shows that when a semiconductor absorbs photons of energy larger than the gap of the semiconductor, when an electron is transferred from the valence band to the conduction band, there occurs an abrupt increase in the absorbency of the material to the wavelength corresponding to the band gap energy. The relation of the absorption coefficient (α) to the incidental photon energy depends on the type of electronic transitions.

When in this transition, the electron momentum is conserved, the transition is direct, but if the momentum does not conserve this transition, it must be attended by a photon which is an indirect electronic transition.[71] Energy band gap studies of these materials were reported using absorption spectra. Absorption spectra of CuO NPs show a strong fundamental absorption edge approximately 219 nm due to direct transition of electrons. The functional property of FTIR spectra study on an absorbed band of approximately 640 cm^{-1} shows the characteristic band of monoclinic phase of pure CuO similar to that obtained in the literature. The crystal phase of CuO NPs XRD pattern is consistent with all diffraction peaks; the sharp observed planes (110), (-111), (111), (202), (020), (220), (-113) and (022) ratify the monoclinic phase of CuO NPs. Generally, various CuO nanostructures including CuO NPs ,1D CuO nanowires/rods/ tubes, 2D and several complex 3D CuO

nanostructures have been synthesized ecofriendly and synthetically. Normally, morphologies of the synthesized CuO nanostructures can be controlled by selecting certain types of structure-directing and dispersing modifying agents. A brief summary of the obtained CuO nanostructures that are synthesized by using various techniques with or without different additives is presented in table 1 and table 2.

Table 1
Summary of various synthesizing methods, precursors, size, morphology and applications of CuO NPs

Method	Precursors and additives/reagents/solvents	Size & shape	Application
Green synthesis solution combustion[5]	*Tinospora cordifolia* water extract	Sponge like structure, average crystallite sizes 6–8 nm	Photocatalytic, Antioxidant and Antibacterial
Thermal decomposition[11]	Cu-oxalate	different shapes and sizes with average crystalline size 21 and 14nm	photocatalysts
Thermal decomposition[12]	Sodium montmorillonite clay, Na_2CO_3, $CuSO_4.5H_2O$, Tetra- ethyl orthosilicate surfactant cetyltrimethyl ammonium bromide (CTABr), Ethanol, ammonia	Crystalline (5–10 nm)	Photocatalysis
Simple precipitation method[14]	Cu $(NO_3)_2 \cdot 3H_2O$, $(Na_3C_6O_7H_5 \cdot 2H_2O)$, $(C_4H_4Na_2O_6)$, $(CH_3COONa \cdot 3H_2O)$, NaOH, acetic, citric and tartaric	800–900 ~ 1,500 800–900 400–500 nm & Leaf-shaped, Flower-shaped, Urchin-shaped, Oatmeal shaped respectively.	Catalytic
Precipitation[15]	Triphenylphosphine oxide	Spherical shaped 8 nm	photocatalytic
Precipitation technique[16]	Copper (II) acetate and sodium hydroxide	Crystalline nature, average diameter 23 nm	Antimicrobial
Sol–gel[18]	$CuSO_4.5H_2O$, NaOH, distilled water	Nano flake like in structure	Antibacterial
Sol–gel and spray pyrolysis methods[20]	Cu $(CH_3COO)_2$, C_2H_5OH, water	spherical arrangement average size 44 nm	Antimicrobial
Simple-Wet Chemical[21]	Cu $(NO_3)_2 \cdot 3H_2O$, NaOH	Nanosheets of average widths (58 51 50) average length 289 268 to 264	Photocatalytic and catalytic
Reflux condensation[22]	Cu $(NO)_3 \cdot 3H_2O$, NH_4OH and methanol	Flower-shaped hierarchical CuO microspheres	Photocatalytic
Chemical bath[23]	Cu $(NO_3)_2$.$3H_2O$), NaOH	Flowers-like average diameter of 4–5 μm and petals-like 1.5–2 μm CuO NSs	Catalytic
Solution combustion[25]	(Cu $(NO_3)_2$), NH_2CH_2COOH	nanoflower thickness around 50 nm.	Photocatalytic
Simple solution[26]	$CuCl_2.2H_2O$, C_2H8N_2 and NH_4OH	Cocoons shaped diameters at the center and corners ~70 ± 5 nm and 30± 5 nm respectively.	Photocatalyst
Solution phase chemical method[27]	$CuSO_4 \cdot 5H_2O$, ethanol and water	sheet-like nanostructures, average diameter of about 15 nm	photocatalytic
Solution phase method[28]	$CuSO_4 \cdot 5H_2O$, polyethylene glycol (PEG- 10,000)	Sheet-like architecture with the length and width of 250–350nm and 200 ± 20nm	Photocatalytic
Green and chemical method[29]	Azadirachta indica, Hibiscus rosa-sinensis, Murraya koenigii, Moringa oleifera, Copper acetate tetrahydrate, NaOH wereand Tamarindus indica	Spherical average size of 9.8 and 10.77 nm. nm for green synthesised CuO NPs and 36.33 nm chemically synthesised NPs.	antioxidant and anticancer
Biosynthesis[30]	(brown alga) Bifurcaria bifurcate, copper (II) sulfate	dimensions 5–45 nm of spherical CuONPs	Antimicrobial
Wet chemical[31]	(Zn $(NO_3)_2 \cdot 6H_2O$), 2-methylimida-zole $(C_4H_6N_2)$ (NaOH), $(Cu(CH_3CO_2) \cdot 2H_2O)$	Cubic shape ~80nm	Photocatalytic

Colloidal gas aphrons (CGA)[36]	Cu $(NO_3)_2$, NaOH, Deionized water	Core-shell structure of 15–30 nm average crystallite size	Photocatalytic, Antioxidant and Antibacterial
Green route[37]	Dry black beans extract, $CuSO_4^{-}.5H_2O$	Spherical, average size 26.6 nm.	Anticancer
Phytogenic[38]	*flowers of A. elaeagnoidea, (Cu $(NO_3)_2.3H_2O$) and 4-nitrophenol (4-NP)*	Spherical shape between 36 to 54 nm.	Catalytic
Microwave[39]	$CuSO_4$.$5H_2O$, L-arginine and NaOH.	2-dimensional leaf-like morphology of dimensions of approximately 350–450 nm in length and 60–90 nm in width	Photocatalyst
Microwave Hydrothermal[44]	Cu_2Ooxide, Cu $(NO_3)_2$ $3H_2O$, NaOH and NH_4OH	Crystallite size spherical shape, agglomerate of larger plates 14.23 &13.78 nm respectively	Photocatalyst
Hydrothermal[45]	copper acetate dehydrate, NaOH, tri-sodium citrate	Nano leaves of average 13–17 nm sizes	photocatalytic
Hydrothermal-assisted solution[46]	copper nitrate, hexamethylenetetramine (HMTA) solution, NaOH	Similar to a carambola of $\sim 1\mu$ m in length and 300 nm in width Spindly CuO microparticles of thickness of ~5 nm	photocatalytic
Planetary Ball Mill[48]	Copper oxide powder, Acetone and ethyl acetate	Monoclinic,82,116nm	Catalytic
Solvothermal[49]	$Cu(Ac)_2.H_2O$, N,N-dimethylformamide (DMF), polyvinyl pyrrolidone (PVP) , carbon nanotubes	Fined hexapod nanostructures with average diameter of 1.2 μm	Photocatalysis
Thermal oxidation[50]	Cu foils, acetone and isopropanol	Nanowires of more than 10 μm in length and 80 nm in mean diameter.	Photocatalytic
Thermal evaporation and annealing[51]	Cu deposited film	23 nm to 293 nm CuO thin films	photocatalytic
Purchased[52]	Purchased commercially	Spherical < 50 nm	Antibacterial
Emulsion Polymerization/ hydrothermal[53]	$Cu(NO_3)_2.3H_2O$, water/ethanol, carbonaceous saccharide microspheres	Hollow micro- spheres	Catalytic
SPSC[54]	Cu plate, K_2CO_3	Nanoflower	Antimicrobial
Green[55]	Cu $(NO_3)_2.3H_2O$, Abutilon indicum, water	Hexagonal, wurtzite and sponge crystal structure	Photocatalytic, antimicrobial
Eco-friendly[56]	*Tabernaemontana* divaricate leaves	Spherical, 48 ± 4 nmin size	Antibacterial
Green[57]	Bauhinia tomentosa leaf extract, Copper sulphate, nutrient agar	Spherical shaped nanoscale average crystallite size of 22e40nm	antibacterial action
Eco friendly[58]	walnut leaf, Cu $(NO_3)_2$, Dimethylsulfoxide (DMSO), methanol, ethanol, nutrient agar	Spherical average size 80 nm	antioxidant
Biofabrication[59]	Andean blackberry fruit (ABF) and leaf (ABL); and Cu $(NO)_3$	Spherical and 43.3 and 52.5 nm average particle size	antioxidant
Laser Ablation in Liquid[63]	Copper metal pellets	8–35nm diameter, colloidal nanoparticles (NPs) of spherical and highly aggregated metal oxide NPs	Antimicrobial
Eco-friendly[64]	Eichhornia crassipes leaf extract, NaOH	Spherical average range of 20-22 nm	Antibacterial
Microwave heating (Green synthesis)[65]	$CuSO_4.5H_2O$, NaOH, glutamic acid	2D CuO NLs having an average length and width of ~720-800 nm and ~136-160 nm respectively.	Catalyst

Thermal plasma technology[66]	CuO, Cu, Cu_2O, ZnO and Ag	Equi-axes of spherical shape average 20–95nm	Antimicrobial
Green Synthesis[67]	NaOH	Spherical shaped particles with 2–69 nm size	Antiviral Activity
Ultrafiltration Surface Contact[68]	Cu $(NO_3)_2 \cdot 3H_2O$, NaOH	144,50,32 and 14 nm (commercial & grounding CuO, hydro-thermal and UMSCM, respectively	Catalytic
Simple Synthesizing Method[71]	$CuCl_2$, Polly ethylene glycol (PEG-400), NaOH	17.95 nm (350ºC) and 45.25 nm (800ºC) respectively. spherical in shape	Photo catalytic
Chemical Precipitation[72]	$Cu(CH_3COO)_2.H_2O$ glacial acetic acid, $NaBH_4$, acetic/citric/tartaric acid, NaOH	Rod, spherical, star- and flower-shaped. Diameter, 20–30, 10–15, 10–20 & 60–80 nm respectively.	Catalytic
Surfactant-Free Chemical Solution[73]	(H_2NCH_2COOH), $CuCl_2 \cdot 2H_2O$, LiOH, ethanol	Microdots (100 nm to 350 nm)	Photocatalytic
Eco-friendly[74]	Copper sulphate, Water, NaOH	Nano sheets	Photocatalytic
Solution phase[75]	$CuSO_4 \cdot 5H_2O$, cetyltrimethylammonium bromide (*CTAB)*, NH_4OH, NaOH	Nanosheets of average size about 23 nm	Photocatalytic

Table 2
Summary of Common synthesis methods for CuO nanoparticles

Method	Advantages
Electrochemical method[13]	A simple, rapid, one-pot and cost effective approach which usually involves the assembly of two- or three-electrode cell system.
Solution combustion synthesis (SCS)[25]	• A versatile, simple, rapid and single step process, which involves a self-sustain ed reaction in homogeneous solution of different oxidizers and fuels.
Solution phase[28]	Simple, economically viable
Green synthesis[30,65]	• Use of non-toxic, environmentally benign reactants and solvents and releases no unwanted by-products and pollutants. • Eliminate the use of expensive chemicals, consume less energy and generate environmentally benign products and by products Nanoparticles using marine algae is that they are quite stable in solution
Microwave[65]	• Faster, energy saving, environmentally benign route for the synthesis of various nanostructure
Laser ablation[63]	• Simple, inexpensive and possesses several advantages over traditional methods; hence, the nano- materials can be produced with controlled size and properties and without contamination
Hydrothermal / solvothermal[76-80]	• Fabrication of inorganic and metal-organic nanomaterial, including oxides; Group III–V, II–IV and VI elements; MOFs; and transitional metals a) chemical reaction kinetics are greatly increased with a small change in temperature, b) new metastable materials can be created, c) the final products of the materials are of high purity even from impure feedstocks, d) it is cost-effective with no need for precipitating agent, (e) it is eco-friendly, and e) hybrid hydroxylated clays and zeolite cannot be prepared by any other synthesis method • Producing a large number of nanomaterials at a relatively low cost and yielding highly crystalline nanocrystals (NCs) with well-controlled dimensions
Reflux condensation[81]	• Economical, environment friendly, large scale production of nanomaterials with well-defined size and shape and performed at relatively low temperature (< 100 °C) without the use of any expensive equipment. The
Sonochemical[82]	• Achieve the product formed which is made up to fine particles of nanometer dimension • Can generate smaller size range and higher surface area than those reported by other methods

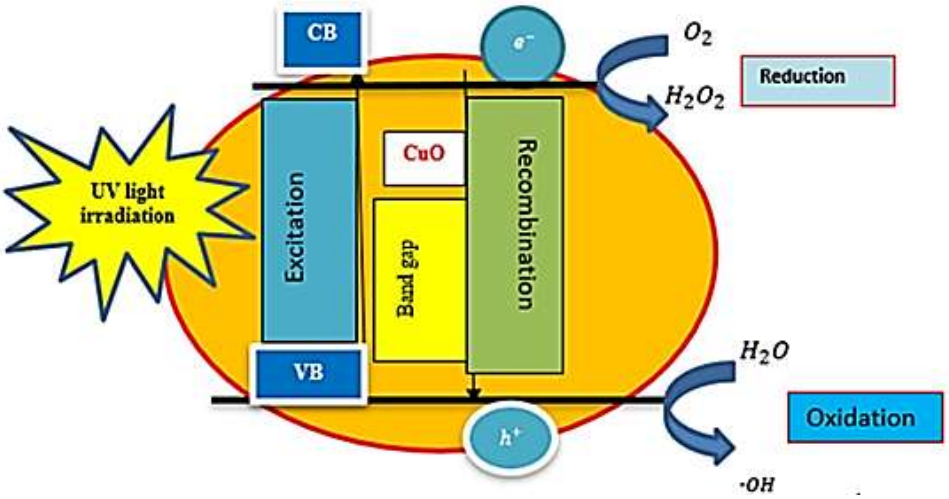

Fig. 12: Typical schematic representation of the photocatalytic dye degradation mechanism under UV light in presence of CuO

Photocatalytic applications of CuO NPs: Photocatalyst is a material that is capable of absorbing light and producing electron–hole pairs that enable chemical transformations of the reaction participants and regenerate its chemical composition after each cycle of such interactions. There are two types of photocatalytic reactions i.e. homogeneous photocatalysis and heterogeneous photocatalysis. The significant features of the photocatalytic system are the desired band gap, suitable morphology, high surface area, stability and reusability. Metal oxides such as oxides of vanadium, chromium, titanium, zinc, tin and cerium having these characteristics follow similar primary photocatalytic processes such as light absorption which induces a charge separation process with the formation of positive holes that are able to oxidize organic substrates.[84-86]

In this process, a metal oxide is activated with either UV light, visible light or a combination of both and photo excited electrons are promoted from the valence band to the conduction band forming an electron/hole pair (e^-/h^+). The photogenerated pair (e-/h+) is able to reduce and/or oxidize a compound adsorbed on the photocatalyst surface. The photocatalytic activity of metal oxide comes from two sources;
I. generation of ·OH radicals by oxidation of OH^- anions,
II. generation of O_2^- radicals by reduction of O_2.

Both the radicals and anions can react with pollutants to degrade or otherwise transform them to lesser harmful byproducts. The physicochemical properties of the metal oxides are crucial for the virtuous photocatalytic performance which are typically size, shape, morphology and composition dependent.[84,85]

Currently, many research efforts are devoted to improving the photocatalytic activity of semiconductor metallic oxides. The photocatalytic degradation mechanism of CuO as presented in figure 12 starts with the absorption of photons (with sufficient energy that equals or exceeds the band-gap energy of the catalyst) through light. The electron becomes excited and jumps to the conduction band, leaving a positively charged hole in the valence band. Besides recombination with the electron, the positively charged hole can oxidize water molecules to form hyper-reactive hydroxyl free radicals $(OH)^*$, the resulting hydroxyl radicals are the main agent that attack the chemical pollutant molecules or microorganism cells to purify water.

The excited electron can react with a dissolved oxygen molecule to form oxygen radical, which is also active toward organic pollutant. As of our knowledge from the perspective of synthesizing methods of CuO NPs, the synthesis procedure plays a crucial role in controlling the size, the shape of the nanostructure and hence detecting different properties of the material which determine the photocatalytic efficiency of the nanomaterial.

Mechanisms to increase a better photocatalytic material of CuO sheet-like nanostructures synthesized by a facile solution phase chemical method is a closer look of nanothechnology. Compared to commercial CuO powders, it was proposed[28] that the prepared naomatrial is a better photocatalytic degradation of pollutant rhodamine B (RhB) under UV light irradiation. After 9 hrs of UV light irradiation, about 96.7% of RhB was degraded by using CuO sheet-like nano- structures where as only 39.6% of the same dye was degraded by commercial CuO powders. But the study did nothing about repeatiblity of the synthesised CuO nanostructued material. Similarly, better photocatalytic efficiency of CuO nanowires (NWs) than Cu_2O NWs in degradation of methyl orange was confirmed.[50] This is probably depending on the large number of defects induced by the thermal treatment in vacuum due to the formation of a polycrystalline structures Cu_2O and mono-crystalline for CuO NWs.

Motivated by their earlier work, another researcher[66] extended his study to evaluate the catalytic activity of CuO NLs for the reduction of aromatic nitro compounds by $NaBH_4$ which is taken as a model reaction. The p-

nitrophenol (PNP) is reduced using a reducing agent $NaBH_4$ in the presence of the catalyst. When CuO NLs are added, the absorption maximum was observed at 403 nm but gradually decreases with time due to the reduction of PNP and fading the color of the solution. According to the authors, higher rate of photo degradation is due to the following reasons:

i. Due to the special leaf-like morphology of CuO nanoparticles, the exposed surface area is higher than that of spherical CuO NPs.
ii. The formation of amino acid (L-arginine) capped CuO NPs. Due to the presence of arginine on the surface of CuO nanoleaves, the electron–hole re-combination will be hindered.

Improvement of photocatalytic efficiency of CuO NPs: In fact, increasing the amount of the photocatalyst increases the number of adsorbed dye molecules onto the photocatalyst surface, but excess photocatalyst particles in the solution decrease the light penetration and hence reduce the photo degradation rate.[87] This is due to the aggregation of solid particles when a large amount of photocatalyst is used.[88] H_2O_2 is one of the most widely used green oxidants which typically requires a catalyst for activation into more reactive oxidizing intermediates.[89] In the degradation of dyes, the role of H_2O_2 is explained by many aouthors. The necessity of H_2O_2 when flower-shaped hierarchical CuO microspheres were synthesized, had been discussed.[22]

In combination with H_2O_2, under UV light irradiation the degradation of MO and MB dyes increased sharply. Concentration also affects the adsorptive and reactive processes in various manner. Adsorption of dye molecules on the catalyst surface hinders the competitive adsorption of OH^- ions i.e. with the increase in the dye concentration, more dye molecules are adsorbed on the surface of CuO and reduce the active sites for adsorption of OH^- ions thereby decreasing the generation of $^{\bullet}OH$ radicals. On the other hand, morphology of nanomaterial of the CuO also affects the efficiency of photocatalytic property.

A study[44] on rapid synthesis of CuO NPs with different morphologies using microwave hydrothermal method from two different mineralizing agents (NaOH and NH_4 OH) evaluated photocatalyst performance against RNL azo dye. Accordingly, photocatalytic performance assessed by UV-Vis spectra and an observation through the percentage discoloration of the RNL dye after the adsorption processes show photo degradation or discoloration reached 85% for CuO NPs using Na0H and 93% for NH_4 mineralizing agents respectively.

This may be because the shape of particles also influences the photo degradation. Although the CuO NPs with mineralizing agent of NaOH sample had a larger surface area than the CuO NPs mineralized with NH_4 sample, 23.486 and 11.758 $m^2. g^{-1}$ respectively, the photo degradation of the latter sample was slightly higher representing the morphology of the particular agglomerates which is more influential than the surface area of the catalyst.

The other way to improve photocatalytic efficiency of metal oxide semiconductors is by tuning of their band gap. Most of metal oxide semiconductors are unable to absorb visible light because of their wide band gap. While, small band gap containing semiconductors exhibit fast recombination phenomenon, photo-generated holes and electrons are unable to act efficiently for photocatalytic conversion. The tuning can be done by delaying the recombination time by monitoring the defect density in the semiconductor lattice, trapping the photo-generated electrons or holes by introduction of co-catalyst, or doping of hetero-atom and functionalization of photocatalysts.[90-92]

The band gap energy different shapes of CuO like the flower, boat, plate and ellipsoid-like are calculated as 1.425, 1.429, 1.447 and 1.371 eV respectively (Table 3). It is known that the light harvesting process is strongly dependent on the surface morphology and structure of photocatalysts. As summarized in table 3, one of the effects of the morphology of CuO nanostructure and its band gap is the type of synthesizing method. Important role is to control the photocatalytic activity of nanomaterials and it should be in an appropriate range to absorb the visible light. Even though it is larger value, it shows excellent photocatalytic activity for the degradation of MO under UV irradiation.

This is due to strong quantum size confinement effect. Studies show that CuO is intrinsically a p-type semiconductor with a low band gap (1.2–2.0 eV), indicating its potential in photo detection and optical switching applications in the visible range in which other metallic oxides with their larger band gaps fail to perform.[93,94]

Table 3
Band gap energy of CuO NPs synthesised by different methods

Synthetic technique	Band gap in eV.
Green[5]	4.48 and 3.330
Hydrolysis method[17]	1.59
Environmentally friendly[55]	3.37
Solution combustion[25]	3
Solution phase chemical[27]	2.31
Solution phase method[28]	1.31
Wet chemical	2.05

CuO photocatalyst having large surface area is favorable for absorption of large number of photons which generate photo excited electron– hole pairs. The increase in band gap also facilitates absorption of photons in the visible region and hinders exitonic recombination to favor photocatalytic activity under direct sunlight. There are many semiconductor support materials that are used to enhance the properties of nanomaterials. Usually these are classified by their chemical nature and these can be organic or inorganic supports. Unfortunately, the metal oxide NPs with high specific surface areas and surface energy tend to aggregate together resulting in decreasing the catalytic respondence.

Therefore, it is necessary to anchor metal oxide NPs to some supporters to decrease the agglomeration and enhance their stability. But in the preparation of nanoparticle material, the choice of supporting materials used to enhance the photocatalysis property is the most important factor. In one interesting example efforts to produce CuO NPs materials,[25] it was observed that the citric acid and glycine to be ideal fuels as they form complexes with the metal ions facilitating homogenous mixing of the cations in solution.

Due to the presence of these organic materials used as fuel, the crystalline nature and the shape factor of the CuO are the main factors for the enhanced photocatalytic activity with respect to bulk materials. This shows that even though the prepared CuO nanoflowers exhibit a higher band gap of 3 eV, it shows excellent photocatalytic activity for the degradation of MO under UV irradiation. Synthesis involving the combination of CuO with other inorganic materials is also a common approach for photocatalyst applications. CuO NPs deposited with ZIF-8[33] exhibited significantly increased photocatalyst with higher ability for dye degradation.

Taking pure rhodamine 6G (Rh6G) dye solution without a catalyst and when 25 mg of CuO NPs/ZIF-8 nanocomposites catalyst is added on 60mL aqueous solution of Rh6G (12.5 ppm) at room temperature, the photocatalytic activity of CuO NPs/ZIF-8 nanocomposites is estimated by monitoring the successive decrease in absorption intensity of Rh6G at 526 nm as a function of reaction time.

The gradual decrease in the characteristic absorbance at λ_{max} 526 nm corresponds to the dye concentration in solution. After sunlight irradiation for 105 min, the CuO NPs/ZIF-8 nanocomposites were photocatalytically active, but the photodegradation rate of Rh6G dye was not very fast in absence of any externally added oxidant. This may be due to relatively fast recombination of photogenerated electrons and holes of CuO NPs/ZIF-8 nanocomposites. The catalytic photodegradation efficiency of CuO NPs/ZIF-8 nanocomposites significantly enhances when 1 mL of H_2O_2 is added.

In a related work, CuO NPs doped with zeolite X were examined as a photocatalyst in the photo decolorization of methyl blue dye under sunlight. The CuO/zeolite bed plays a significant role in the photodegradation process while zeolite X whereas pure CuO does not show photo decolorization efficiency.[94] With a similar concept, a study[46] in the presence of approximately 0.01 M H_2O_2 shows irradiation by a 100 W halogen tungsten lamp as source of light. CuO NPs are very stable and could be recycled without considerable loss of activity.

Moreover, the synthesised material can also be used to photodegrade other pollutants like MO, MB, erosin B and p-nitrophenol under identical conditions. Stability and reusability of the carambola-like CuO are examined by repetitive use of the catalyst. With this regard, the catalyst did not exhibit a significant loss of activity after five photodegradation cycles of RhB.

Hence, addition of H_2O_2 improved the photocatalytic activity of the spindly CuO micro-particles. Sohrabnezhad and Takas[12] conducted a study of preparation and characterization of porous clay heterostructure (PCH) as a high-surface area sup- port for CuO NPs for the preferential oxidation of MB under visible light in the absence of H_2O_2.

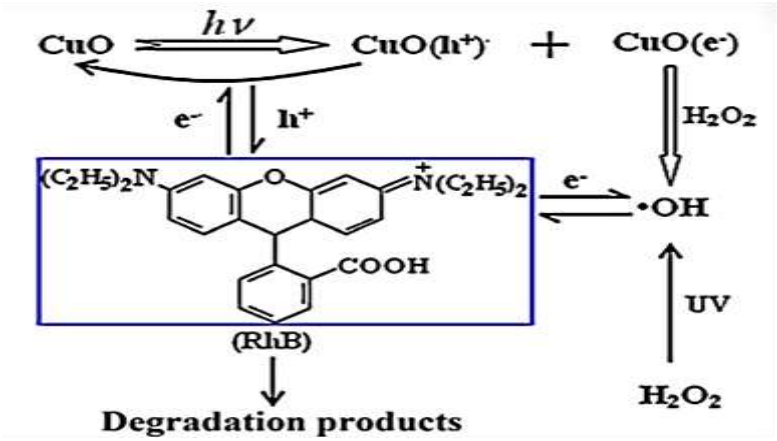

Fig. 13: Scheme of photodegradation of RhB in the presence of spindly CuO and H_2O_2 under irradiation by a halogen tungsten lamp[46]

The study shows the enhancement of CuO NPs loaded in PCH on in visible irradiation in the degradation rate of MB. The CuO nanoparticles, CuO– sodium montmorillonite clay (MCM), CuO–MMT and PCH did not have significant degradation efficiency. Hence, the aluminum atoms and mesoporous material in PCH showed an important role in the degradation process.

Literatures show that the addition of H_2O_2 enhances the photocatalytic activities of many semiconductors such as TiO_2,[95] CdS,[96] and ZnO.[97] Furthermore, other workers[98,99] clarified the reason for the mechanism of this enhancement which is mainly accredited with two reasons. First, compared with molecular oxygen, H_2O_2 is a better electron acceptor. It can be converted to •OH radicals after accepting the electrons. Second, H_2O_2 may be photolytically split directly to produce •OH under UV radiation of up to ∼370 nm.[100] The mechanism for the photodegradation of RhB when spindly CuO employed as shown in figure 13 shows that under simulated sunlight, electrons and holes are generated on the surface of CuO.

The electrons can be scavenged by H_2O_2 to produce •OH which lowers the electron–hole recombination rate and thereby increases the hole utilization in the photocatalytic oxidation of RhB. At the same time, •OH generated from the reduction of H_2O_2 by the photo-generated electrons and the direct decomposition of H_2O_2 by UV light can also directly oxidize RhB, which further enhances its decomposition.

In addition to effects of adding surfactants and matrices agents into the CuO starting solution on the growth, size and morphology of the obtained CuO nanostructures, the efficiency of photocatalytic property of CuO NPs can be improved by testing different synthesis methods which is directly related to surface morphology.

The oxidation reaction of the particles,[69] had been made with UMSCM, hydrothermal and grounding method as well as a commercial for catalytic comparison. CuO prepared with UMSCM shows better catalytic performance than the other three methods. This is because the activities of the catalysts are controlled by their particle sizes and defects.

The defect of p-type semiconductor oxidant CuO is mainly in the vacancy of the copper ion in the cation sub-lattice, which accelerates the surface adsorption rate of O_2 molecules through defects. Defects are beneficial to the diffusion of ions and atoms, which enhance catalytic activity. Except commercial CuO, the rest three types of CuO have large amounts of defects.

As a result, these three types of CuO have higher catalytic activity than the commercial one. Among them, the CuO prepared by UMSCM has the smallest particle sizes thickness, the largest specific surface area and thus the highest activity to improve the catalytic performance of CuO, nanometer-sized particles. Surface area is important as a measure of available active surface sites for photocatalytic reactions.

The effectiveness of the CuO nanostructures as catalysts for the Rochow reaction of direct synthesis of dimethyldichlorosilane ($(CH_3)_2SiCl_2$) has been confirmed. Cu_3Si (η phase) is the active catalyst leading to selective formation of $(CH_3)_2SiCl_2$. The catalytic activity is directly related to the amount of Cu_3Si phase formed during the reaction. The finding of this study shows that the effect of CuO nanostructure geometries is distinct. Hence, among the four prepared catalysts, with leaf, urchin, flower and oatmeal-shaped morphologies, the leaf shaped CuO nano structure is the best catalyst performed among all the CuO nanostructure catalysts.

This is due to high specific surface area that facilitates the adsorption of methyl chlorosilanes (MeCl) and contact with Si, in addition to this, the exposed O^{2-}-terminated {001} plane that imparts the strongest adsorption ability to the catalyst for oxygen species and enhanced reducibility. Both these factors contribute to the formation of more Cu_3Si species, thus enhancing the catalytic activity for dimethyl (M2) production. Similar report[101] showed that copper catalysts employed in the direct synthesis reaction are in actuality catalyst precursors nanosized copper catalyst precursors depending upon the method and conditions of its preparation.

Factors affecting photocatalysis property of CuO NPs: Even though photocatalytic activity is affected by the properties of a photocatalyst as well as the reaction conditions (pH, concentration, illumination power temperature stability etc.), it is noteworthy to mention that the fabrication process optimization of important factors such as pH, the quantity of leaf extract, copper precursor concentration, incubation time and temperature on the formation of CuO-NPs surface area and the material quality,[76] suitable band gap energy and chemical stability over long rang irradiation time, (crystallinity, size shape and/or natural defects) can determine the photocatalysis efficiency of nanomaterials.

Zaman et al[23] indicated comparing shapes of flowers-like and petals-like CuO NSs and the degradation of rhodamine B in the presence of H_2O_2 and organic dye MB. CuO NSs of petals shape show stronger catalytic activity in the degradation of the organic dyes than flowers like CuO NSs. This may be due to the higher specific surface area of CuO petals. These CuO NSs have the potential to be used as a room temperature catalyst without using any specific light source.

According to a study,[53] in the absence of CuO hollow microspheres catalysts ammonia-borane (AB) is stable in air and in aqueous solution at room temperature. But at different temperatures 30, 35, 45 and 60 ^{o} C in 30mL of H_2O, the hydrolytic dehydrogenation of AB is performed at different

volume of hydrogen using the prepared CuO hollow microspheres (Figure 15).

With this regard, the thickness of the shells and the size of the pores on the hollow spheres are mainly responsible for the hydrogen releasing rate although other factors may also need to be considered. Even though the active sites exist on both inside and outside surfaces of the hollow spheres, the thicker are the shells, the smaller is the surface area, the less active sites may be due to smaller pores and it is more difficult for the AB molecules to pass through them to reach the inside surface of the hollow spheres especially when the AB molecules are hydrated in aqueous solutions. In order to obtain the activation energy (E_a) of the AB hydrolysis catalyzed by the more efficient CuO, the hydrolytic reaction was carried out at four different temperatures (30, 35, 45 and 60 ^oC). Figure 14 shows that when temperature is increased; volume of hydrogen released from AB increased.

The synthesis procedure or technique plays a crucial role in controlling the size, the shape of the nanostructure and hence detecting different properties of the material. The chemical structure of a dye also has tremendous effect on photocatalysis performance. Currently many studies are emerging just to test the photocatalysis efficiency of a nanomaterial using different organic dyes. The photocatalytic activity of CuO NPs for RhB and MB degradation under visible light irradiation has been investigated.[29] It is obvious that under controlled experiments, no degradation of MB and RhB was observed during the photolysis and catalysis in dark conditions.

But under visible light irradiation, rate of the reaction for MB degradation is faster than RhB degradation. A similar study[102] showed that the alkyl side chain in RhB decreases its solubility in water, hereafter the structure of dyes plays a major role in the adsorption of dye molecules at the nano catalysts surface.

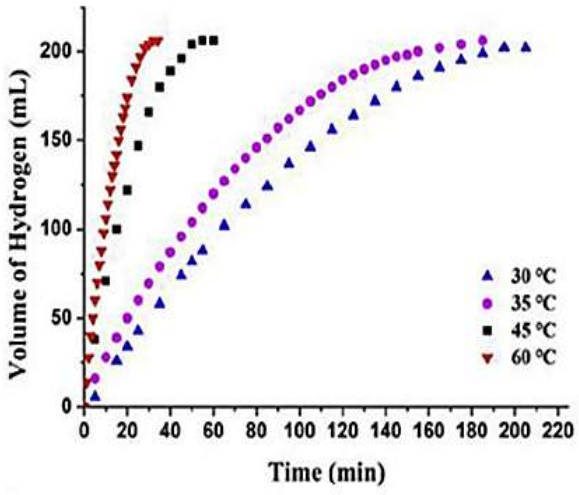

Fig. 14: Time plots of catalytic dehydrogenation of AB over the CuO hollow spheres catalysts at different temperatures[53]

Moreover, Huang et al[74] used CuO micro rods to be used as catalyst to photodegrade RhB, MO, MB, eosin B and p-nitrophenol comparing to commercial CuO powders. The outstanding photocatalytic properties in the degradation of RhB were observed by the prepared porous CuO micro rods than the commercial.

Currently the stability of newly synthesized catalyst is a serious issue in heterogeneous photocatalysis since some of the photocatalytic materials are not stable upon prolonged light irradiation. For instance, CdS undergoes photo-corrosion in the long run photocatalytic reactions.[103]

Therefore, to examine the stability of prepared CuO nanosheets, XRD analysis is carried out for fresh CuO sample and reused CuO sample (after three photocatalytic cycles) as in figure 15. There is no noticeable change in the phase of CuO sample, which designates that the prepared CuO catalyst is stable after three cycles. Hence, there is no much change in the degradation efficiency of CuO catalyst after three cycles. It was reported that CuO hexapod nanostructures exhibit superior property on photocatalytic decomposition of phenol than commercial CuO.[49] This is mainly due to the unique porous hexapod nanostructures.

In addition, the as-prepared hexapod CuO nanostructures show great potential as visible-light-driven photocatalyst while other nanomaterials including pure TiO_2 nanoparticle or nanotube and CdS only take effect under UV-light. The development of photocatalytic experiment was carried out by varying of catalyst amount and initial concentration of Reactive Black-5 (RB-5) dye supporting CuO nanosheets as effective photocatalysts under visible light.[27]

It is obvious that to see how we can control the photodegradation of the material for each temperature, photocatalytic degradation of a dye should be carried out on each as-synthetized NPs at range of different annealing temperatures under same irradiation condition. The photocatalytic activity of CuO NPs on the degradation of various organic toxic compounds under UV and visible light is studied using different measuring parameters like annealing temperature,[21,51] shape of CuO NPs.[14,25,44,72] Photodegradation of Rh-B in spherical shaped CuO NPs annealed at 350 ^oC is relatively more active than the pebble shaped CuO annealed at 800 ^oC.

This shows that the homogenous and heterogeneous catalytic efficacy of phytogenic CuO NPs also depends on the size of the particles.

PVP has been found to have impact[21] on morphological, structural, optical, catalytic and photocatalytic efficiency in the preparation of the nanomaterial. Among various amounts of PVP (0, 0.1 and 0.2 g) in the solution, CuO nanosheets prepared using an optimal PVP concentration show superior photocatalytic activity for degradation of MB and MO dyes.

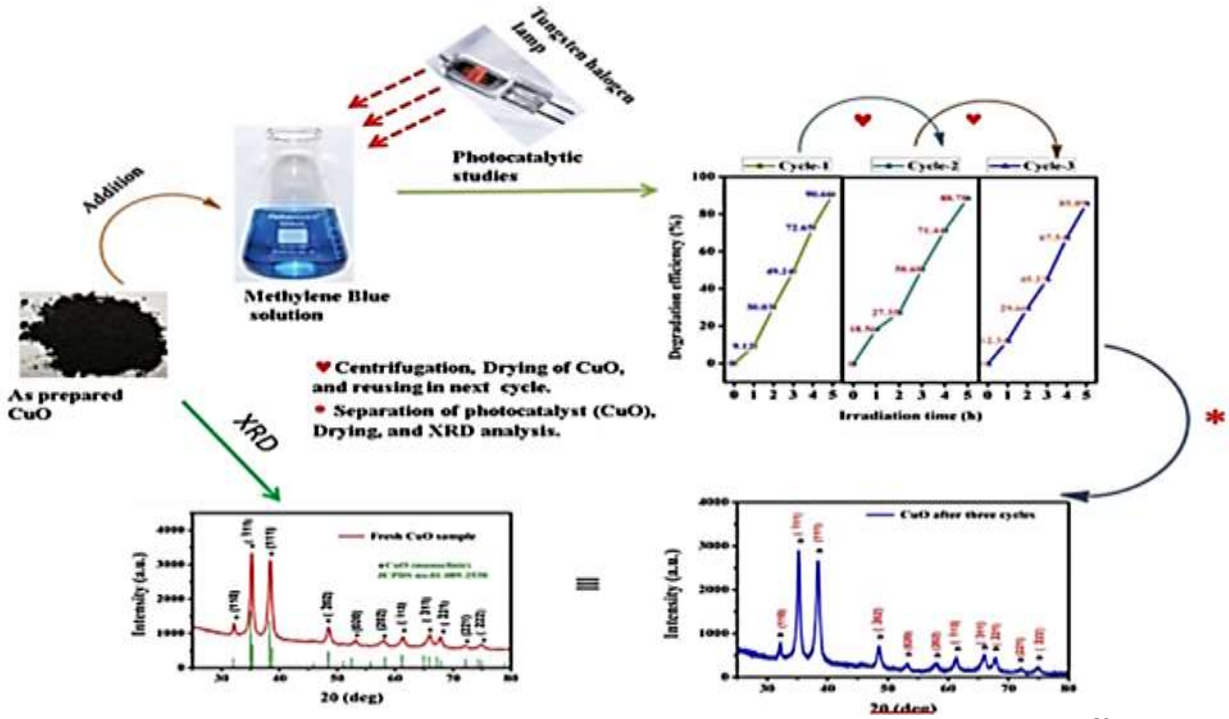

Fig. 15: A detailed depiction of stability and reusability of CuO nanosheets catalyst[29]

It also exhibited a highly enhanced catalytic efficiency for the transformation of 4-nitrophenol (4-NP) into 4-aminopheol (4-AP). CuO nanosheets with highest PVP completely degraded MB and MO dyes in 150 and 180 min respectively.

In addition, complete transformation of 4-NP into 4-AP by CuO nanosheets occurred in just 5 min. This may be due to narrow band gap, smaller crystallite size, improved light utilization and high surface area of CuO nanosheets which enhanced the stability of the photocatalytic activities.

In spite of the extensive efforts to increase photocatalytic efficiency of CuO in the visible region, it remained quite low. This is a question that was addressed recently highlighting challenges associated with the application of photocatalysis. Normally, two or more phases are involved in a photocatalytic reaction but a light source and a semiconductor material are used to initiate the photoreaction while the catalyst system can simultaneously carry out oxidation and reduction reactions using long wavelength, UV light as well as sunlight.

Among these attempts,[55] it was reported that stepwise effective degradation of organic toxic dyes such as Acid Black 210 occurs under sunlight irradiation. In the first step, cupric oxide nanostructure comes in contact with light creating a photo-generated electron and a hole. The photo-generated electron reacting with oxygen molecule to form superoxide free radical is the second step. Finally, the hole reacts with water and hydroxyl ions to produce highly mercurial hydroxyl radicals. These superoxide free radicals and hydroxyl free radicals react violently with Acid Black 210 organic dye and decompose/ decolorize it in the next step. This may be the degradation/decomposition rate of the organic dye which totally depends on morphological and crystal structure of the photochemical catalyst. The active sites of photocatalysts can be increased by increasing surface area and crystalline structure; these in turn increase the effectiveness of photocatalytic reactions by separating electron-hole pairs.

The effect of photo degradative activity of known amount of CuO NPs can be evaluated against concentrations of dye, or pH of the dye. Due to many reasons, increasing the dye concentration may decrease the photodegradation efficiency of NPs. Even though the photodegradation efficiency depends on the formation of hydroxyl radicals, the effect of pH on photocatalytic degradation has huge effect.

In study of such type of effects,[5] it was successfully demonstrated that the degradation of MB is at fixed levels of dye and catalyst by changing pH from 2 to12. The results show that the photodegradation efficiency decreases with increase in pH. At low pH value (pH=2) the photodegradation efficiency was 91.23%. When the pH value of MB dye solution increased from 2 to 4, the photodegradation efficiency of the nanomaterial almost increased to 96.93% but decreased with further increase in pH. In other way, with increasing of catalytic load, the efficiency increases, but increase in catalytic load did not show any effect on the photodegradation efficiency.

This leads to increased number of active sites available on the catalyst surface for the reaction due to enhanced catalyst load, which in turn increased the number of holes and hydroxyl radicals. Thus, the photocatalytic activity decreased due to the increment of the electrostatic repulsion

between CuO and anionic MB. In addition, the increase of pH may increase e^-/h^+ recombination rate and subsequently decrease the photocatalytic activity.[105] The best pH value for the efficient photodegradation of MB blue was 4 at which the positively charged CuO and negatively charged MB molecules attract each other and photocatalytic oxidation occurs very effectively.

Conclusion

Even though various synthetic approaches for CuO NPs are reported, due to the advancement of nanoscience and technology it is necessary to evaluate the cost effectiveness, the availability of resources and performances in different applications. Hence, comparing and knowing the current status of the research area of CuO NPs will provide huge information and give various opportunities for investigation of new innovative approaches.

In this review, we observe that post reaction characterization is important to evaluate the recyclability of synthesised CuO NPs. In addition, most of the studies focused on the degradation of the dye but studies on testing the toxicity of CuO NPs after degradation and antimicrobial activities are still rare. Although there is a greater consensus on the antimicrobial activity of CuO which is due to the release of Cu^{2+} ions, the exact mechanism of action is still unclear. Numerous already existing synthesis methods provide a rich base that may fuel research devoted to such applications. This is particularly important keeping in mind that the type of the synthesis affects properties like size, shape, morphology, dispersity, presence and type of stress and defects in the crystal which in turn determines their interaction with organic dyes and microbial cells.

The reactivity may also be determined by their solubility and degree of agglomeration. For observation, many researchers used UV-vis spectroscopy for photocatalytic studies, only few researchers used GC-MS for similar purpose. We conclude that, even though the current synthetic pathways are encouraging for the large-scale production of the materials, the control and refinement of particles with the superior properties need to be further explored. At outset, the properties of CuO nanostructures can be improved through various methods outlined, but uniform properties will be key to the development of real-world applications.

Acknowledgement

Authors are grateful to Adama Science and Technology University for the support towards this work.

References

1. Chatzimitakos T.G. and Stalikas C.D., Qualitative Alterations of Bacterial Metabolome after Exposure to Metal Nanoparticles with Bactericidal Properties: A Comprehensive Workflow Based on 1 H NMR, UHPLC-HRMS and Metabolic Databases, *J. Proteome Res.*, **15**, 3322–3330 **(2016)**

2. Ananda Murthy H.C., Abebe B. and Tegene D.Z., Areview on green synthesis and applications of Cu and CuO nanoparticles, *Mat. Sci. Res. Ind.*, **16**, 252–60 **(2018)**

3. Serpone N. and Emeline A.V., Semiconductor Photocatalysis — Past, Present and Future Outlook, *J. Phys. Chem. Lett.*, **3**, 673–677 **(2012)**

4. Ananda Murthy H.C., Desalegn T., Kassa M., Abebe B. and Assefa T., Synthesis of Green Copper Nanoparticles Using Medicinal plant Hagenia abyssinica (Brace) JF. Gmel. Leaf extract: Antimicrobial properties, *J. Nanomater.*, **2020**, 1-12 **(2020)**

5. Ananda Murthy H.C., Prakash C.H., Buzuayehu Abebe and Kumar Shantaveerayy, Green Synthesis of Cu/CuO and Ag_2O Nanomaterials for Multifunctional Applications, *Current Research in Science and Technology*, **4**, 113-131**(2020)**

6. Das D., Nath B.C., Phukon P. and Dolui S.K., Synthesis and evaluation of antioxidant and antibacterial behavior of CuO nanoparticles, *Colloids Surfaces B Biointerfaces*, **101**, 430–433 **(2013)**

7. Anandan S., Lee G.J. and Wu J.J., Sonochemical synthesis of CuO nanostructures with different morphology, *Ultrason. Sonochem.*, **19**, 682–686 **(2012)**

8. Yuan G.Q., Jiang H.F., Lin C. and Liao S.J., Shape- and size-controlled electrochemical synthesis of cupric oxide nanocrystals, *J. Cryst. Growth.*, **303**, 400–406 **(2007)**

9. Lim Y.F., Choi J.J. and Hanrath T., Facile Synthesis of Colloidal CuO Nanocrystals for Light-Harvesting Applications, *J. Nanomater.*, **2012**, 1–6 **(2012)**

10. Behari J., Principles of nanoscience: An overview, *Indian J. Exp. Biol*., **48**, 1008–1019 **(2010)**

11. Nguyen T.H., Nguyen T.L., Ung T.D.T. and Nguyen Q.L., Synthesis and characterization of nano-CuO and CuO/TiO 2 photocatalysts, *Adv. Nat. Sci. Nanosci. Nanotechnol.*, **4**, 025002 **(2013)**

12. Sohrabnezhad S. and Takas M.E., Synthesis and characterization of porous clay heterostructure intercalated with CuO nanoparticles as a visible light-driven photocatalyst, *J. Iran Chem. Soc.*, **16**, 45–55 **(2019)**

13. Katwal R., Kaur H., Sharma G., Naushad M. and Pathania D., Electrochemical synthesized copper oxide nanoparticles for enhanced photocatalytic and antimicrobial activity, *J. Ind. Eng. Chem.*, **31**, 173–184 **(2015)**

14. Yu Zhang, Ji Y., Li J., Liu H., Hu X., Zhong Z. and Su F., Morphology-dependent catalytic properties of nanocupric oxides in the Rochow reaction, *Nano Res.*, **11**, 804–819 **(2018)**

15. Sharma Aarti and Dutta R.K., Studies on the drastic improvement of photocatalytic degradation of acid orange-74 dye by TPPO capped CuO nanoparticles in tandem with suitable electron capturing agents, *RSC Adv*., **5** 43815–43823 **(2015)**

16. Maqusood Ahamed, Alhadlaq H.A., Khan M.A.M., Karuppiah P. and Al-Dhabi N.A., Synthesis, Characterization and Antimicrobial Activity of Copper Oxide Nanoparticles, *J.*

Nanomater., **2014**, 1–4 **(2014)**

17. Ahmed Mohsen Ismail, Emara M.M., El din Kassem T.S. and Moussa M.A., How assembly matters to catalysis and thermal conductivity mediated by CuO nanoparticles, *Nanotechnology*, **28**, 075705 **(2017)**

18. Pandiyarajan T., Udayabhaskar R., Vignesh S., James R.A. and Karthikeyan B., Synthesis and concentration dependent antibacterial activities of CuO nanoflakes, *Mater. Sci. Eng. C.*, **33**, 2020–2024 **(2013)**

19. Betke A. and Kickelbick G., Bottom-Up, Wet Chemical Technique for the Continuous Synthesis of Inorganic Nanoparticles, *Inorganics*, **2**, 1–15 **(2014)**

20. Etefagh R., Azhir E. and Shahtahmasebi N., Synthesis of CuO nanoparticles and fabrication of nanostructural layer biosensors for detecting Aspergillus niger fungi, *Sci. Iran.*, **20**, 1055–1058 **(2013)**

21. Sahu K., Singh J. and Mohapatra S., Photocatalytic and catalytic removal of toxic pollutants from water using CuO nanosheets, *J. Mater. Sci. Mater. Electron.*, **30**, 6088–6099 **(2019)**

22. Mageshwari K., Sathyamoorthy R. and Park J., Photocatalytic activity of hierarchical CuO microspheres synthesized by facile reflux condensation method, *Powder Technol.*, **278**, 150–156 **(2015)**

23. Zaman S., Zainelabdin A., Amin G., Nur O. and Willander M., Efficient catalytic effect of CuO nanostructures on the degradation of organic dyes, *J. Phys. Chem. Solids*, **73**, 1320–1325 **(2012)**

24. Kim S.H., Umar A., Kumar R., Ibrahim A.A. and Kumar G., Facile synthesis and photocatalytic activity of cocoon-shaped CuO nanostructures, *Mater. Lett.*, **156**, 138–141 **(2015)**

25. Umadevi M. and Christy A.J., Spectr ochimica Acta Part A: Molecul ar and Biomo lecular Spectrosco py Synthesis, characterization and photocatalytic activity of CuO nanoflowers, *Spectrochim. Acta Part A Mol. Biomol. Spectrosc.*, **109**, 133–137 **(2013)**

26. Kim S.H., Umar A., Kumar R., Ibrahim A.A. and Kumar G., Facile synthesis and photocatalytic activity of cocoon-shaped CuO nanostructures, *Mater. Lett.*, **156**, 138–141 **(2015)**

27. Rao M.P., Wu J.J., Asiri A.M., Anandan S. and Ashokkumar M., Photocatalytic properties of hierarchical CuO nanosheets synthesized by a solution phase method, *J. Environ. Sci.*, **69**, 115–124 **(2018)**

28. Wang L.J., Zhou Q., Liang Y., Shi H., Zhang G., Wang B., Zhang W., Lei B. and Wang W.Z., Size effect and enhanced photocatalytic activity of CuO sheet-like nanostructures prepared by a room temperature solution phase chemical method, *Appl. Surf. Sci.*, **271**, 136–140 **(2013)**

29. Rao M.P., Sathishkumar P., Mangalaraja R.V., Asiri A.M., Sivashanmugam P. and Anandan S., Simple and low-cost synthesis of CuO nanosheets for visible-light-driven photocatalytic degradation of textile dyes, *J. Environ. Chem. Eng.*, **6**, 2003–2010 **(2018)**

30. Rehana D., Mahendiran D., Kumar R.S. and Rahiman A.K., Evaluation of antioxidant and anticancer activity of copper oxide nanoparticles synthesized using medicinally important plant extracts, *Biomed. Pharmacother.*, **89**, 1067–1077 **(2017)**

31. Siddiqui H., Qureshi M.S. and Haque F.Z., One-step, template-free hydrothermal synthesis of CuO tetrapods, *Optik (Stuttg)*, **125**, 4663–4667 **(2014)**

32. Aygün S. and Cann D., Hydrogen sensitivity of doped CuO/ZnO heterocontact sensors, *Sensors Actuators, B Chem.*, **106**, 837–842 **(2005)**

33. Chakraborty A., Islam D.A. and Acharya H., Facile synthesis of CuO nanoparticles deposited zeolitic imidazolate frameworks (ZIF-8) for efficient photocatalytic dye degradation, *J. Solid State Chem.*, **269**, 566–574 **(2019)**

34. Raul P.K., Senapati S., Sahoo A.K., Umlong I.M., Devi R.R., Thakur A.J. and Veer V., CuO nanorods: a potential and efficient adsorbent in water purification, *RSC Adv.*, **4**, 40580–40587 **(2014)**

35. Kida K., Okita M., Fujita K., Tanaka S. and Miyake Y., Formation of high crystalline ZIF-8 in an aqueous solution, *Cryst. Eng. Comm.*, **15**, 1794 **(2013)**

36. Banifatemi S.S., Mohammadifard H. and Amiri M.C., A novel method to synthesize copper oxide nanoparticles by using colloidal gas aphrons, *Colloids Surfaces A Physicochem. Eng. Asp.*,**497**, 49735–40 **(2016)**

37. Nagajyothi P.C., Muthuraman P., Sreekanth T.V.M., Kim D.H. and Shim J., Green synthesis: In-vitro anticancer activity of copper oxide nanoparticles against human cervical carcinoma cells, *Arab. J. Chem.*, **10**, 215–225 **(2017)**

38. Manjari G., Saran S., Arun T., Bhaskara A.V. and Devipriya S.P., Catalytic and recyclability properties of phytogenic copper oxide nanoparticles derived from Aglaia elaeagnoidea flower extract, *J. Saudi Chem. Soc.*, **21**, 610–618 **(2017)**

39.Bhattacharjee A. and Ahmaruzzaman M., Facile synthesis of 2-dimensional CuO nanoleaves and their degradation behavior for Eosin Y, *Mater. Lett.*, **161**, 20–25 **(2015)**

40. Rao M.P., Wu J.J., Asiri A.M., Anandan S. and Ashokkumar M., Photocatalytic properties of hierarchical CuO nanosheets synthesized by a solution phase method, *J. Environ. Sci.*, **69**, 115–124 **(2018)**

41. Yemmireddy V.K. and Hung Y., Using Photocatalyst Metal Oxides as Antimicrobial Surface Coatings to Ensure Food Safety-Opportunities and Challenges, *Compr. Rev. Food Sci. Food Saf.*, **16**, 617–631 **(2017)**

42. Tran T.H. and Nguyen V.T., Copper Oxide Nanomaterials Prepared by Solution Methods , Some Properties and Potential Applications : A Brief Review, *Inter. Scholarly Res. Notices*, **2014**, 1-14 **(2014)**

43. Singh J. and Rawat M., A Brief Review on Synthesis and Characterization of Copper Oxide Nanoparticles and its Applications, *J. Bioelectron. Nanotechnol.*, **1**, 1-9 **(2016)**

44. Quirino M.R., Lucena G.L., Medeiros J.A., dos Santos I.M.G.

and de Oliveira M.J.C., CuO Rapid Synthesis with Different Morphologies by the Microwave Hydrothermal Method, *Mater. Res.*, **21**, 1-9 **(2018)**

45. Sonia S., Poongodi S., Kumar P.S., Mangalaraj D., Ponpandian N. and Viswanathan C., Materials Science in Semiconductor Processing Hydrothermal synthesis of highly stable CuO nanostructures for efficient photocatalytic degradation of organic dyes, *Mater. Sci. Semicond. Process*, **30**, 585–591 **(2015)**

46. Li J., Sun F., Gu K., Wu T., Zhai W., Li W. and Huang S., Preparation of spindly CuO micro-particles for photodegradation of dye pollutants under a halogen tungsten lamp, *Appl. Catal. A Gen.*, **406**, 40651–58 **(2011)**

47. Dhand C., Dwivedi N., Loh X.J., Jie Ying A.N., Verma N.K., Beuerman R.W., Lakshminarayanan R. and Ramakrishna S., Methods and strategies for the synthesis of diverse nanoparticles and their applications: a comprehensive overview, *RSC Adv.*, **5**, 105003–105037 **(2015)**

48. Ayoman E., Hossini G. and Haghighi N., Synthesis of CuO Nanoparticles and Study on their Catalytic Properties, *Int. J. Nanosci. Nanotechnol.*, **11**, 63–70 **(2015)**

49. Yang L., Chu D. and Wang L., Porous hexapod CuO nanostructures: precursor-mediated fabrication, characterization and visible-light induced photocatalytic degradation of phenol, *Mater. Lett.*, **160**, 246–249 **(2015)**

50. Scuderi V., Amiard G., Boninelli S., Scalese S., Miritello M., Sberna P.M., Impellizzeri G. and Privitera V., Photocatalytic activity of CuO and Cu_2O nanowires, *Mater. Sci. Semicond. Process*, **42**, 89–93 **(2016)**

51. Sahu K., Choudhary S., Khan S.A., Pandey A. and Mohapatra S., Thermal evolution of morphological, structural, optical and photocatalytic properties of CuO thin films, *Nano-Structures & Nano-Objects*, **17**, 92–102 **(2019)**

52. Ebrahim-Saraie H.S., Heidari H., Rezaei V., Mortazavi S.M.J. and Motamedifar M., Promising antibacterial effect of copper oxide nanoparticles against several multidrug resistant uropathogens, *Pharm. Sci.*, **24**, 213–218 **(2018)**

53. Feng X., Chen X.M., Qiu P., Wu D., Hamilton E.J.M., Zhang J. and Chen X., Copper oxide hollow spheres: Synthesis and catalytic application in hydrolytic dehydrogenation of ammonia borane, *Int. J. Hydrogen Energy*, **43**, 20875–20881 **(2018)**

54. Nishino F., Jeem M., Zhang L., Okamoto K., Okabe S. and Watanabe S., Formation of CuO nano-flowered surfaces via submerged photo-synthesis of crystallites and their antimicrobial activity, *Sci. Rep.*, **7**, 1063 **(2017)**

55. Ijaz F., Shahid S., Khan S.A., Ahmad W. and Zaman S., Green synthesis of copper oxide nanoparticles using *Abutilon indicum* leaf extract: Antimicrobial, antioxidant and photocatalytic dye degradation activitie, *Trop. J. Pharm. Res.*, **16**, 743 **(2017)**

56. Abboud Y., Saffaj T., Chagraoui A., El Bouari A., Brouzi K., Tanane O. and Ihssane B., Biosynthesis, characterization and antimicrobial activity of copper oxide nanoparticles (CONPs) produced using brown alga extract (Bifurcaria bifurcata), *Appl. Nanosci.*, **4**, 571–576 **(2014)**

57. Sivaraj R., Rahman P.K.S.M., Rajiv P., Salam H.A. and Venckatesh R., Biogenic copper oxide nanoparticles synthesis using Tabernaemontana divaricate leaf extract and its antibacterial activity against urinary tract pathogen, *Spectrochim. Acta Part A Mol. Biomol. Spectrosc.*, **133**, 178–181 **(2014)**

58. Sharmila G., Sakthi Pradeep R., Sandiya K., Santhiya S., Muthukumaran C., Jeyanthi J., Manoj Kumar N. and Thirumarimurugan M., Biogenic synthesis of CuO nanoparticles using Bauhinia tomentosa leaves extract: Characterization and its antibacterial application, *J. Mol. Struct.*, **1165**, 288–292 **(2018)**

59. Nomura K., Self-dual Leonard pairs Green synthesis of copper oxide nanoparticles extract assessment and biological properties, *Green Process Synth*, **9**, 557–567 **(2019)**

60. Ren G., Hu D., Cheng E.W.C., Vargas-Reus M.A., Reip P. and Allaker R.P., Characterisation of copper oxide nanoparticles for antimicrobial applications, *Int. J. Antimicrob. Agents*, **33**, 587–590 **(2009)**

61. Nasrollahzadeh M., Atarod M. and Sajadi S.M., Green synthesis of the Cu/Fe3O4 nanoparticles using Morinda morindoides leaf aqueous extract: A highly efficient magnetically separable catalyst for the reduction of organic dyes in aqueous medium at room temperature, *Appl. Surf. Sci.*, **364**, 636–644 **(2016)**

62. Maestri D.M., Nepote V., Lamarque A.L. and Zygadlo J.A., Natural products as antioxidants, *Phytochemistry: Advances in Research*, **8**, 105-135 **(2006)**

63. Singh S.C., Swarnkar R.K. and Gopal R., Laser ablative approach for the synthesis of cadmium hydroxide-oxide nanocomposite, *J. Nanoparticle Res.*, **11**, 1831–1838 **(2009)**

64. Khashan K.S., Sulaiman G.M. and Abdulameer F.A., Synthesis and Antibacterial Activity of CuO Nanoparticles Suspension Induced by Laser Ablation in Liquid, *Arab. J. Sci. Eng.*, **41**, 301–310 **(2016)**

65. Hemalatha S. and Makeswari M., Green Synthesis, Characterization and Antibacterial Studies of CuO Nanoparticles from Eichhornia Crassipes, *Rasayan J. Chem.*, **3**, 838-843 **(2017)**

66. Bhattacharjee A. and Ahmaruzzaman M., Microwave assisted facile and green route for synthesis of CuO nanoleaves and their efficacy as a catalyst for reduction and degradation of hazardous organic compounds, *J. Photochem. Photobiol. A Chem.*, **353**, 215–228 **(2018)**

67. Ren G., Hu D., Cheng E.W.C., Vargas-Reus M.A., Reip P. and Allaker R.P., Characterisation of copper oxide nanoparticles for antimicrobial applications, *Int. J. Antimicrob. Agents*, **33**, 587–590 **(2009)**

68. Yugandhar P., Vasavi T., Jayavardhana Y., Palempalli R. and Maheswari U., Cost Effective , Green Synthesis of Copper Oxide Nanoparticles Using Fruit Extract of Syzygium alternifolium (Wt.) Walp., Characterization and Evaluation of Antiviral Activity, *J. Clust. Sci.*, **29,** 743-755 **(2018)**

69. Zhang C., Bai Y., Yin Y., Gu J. and Sun Y., High catalytic performance of CuO nanocrystals with largest defects, *Korean J. Chem. Eng.*, **28**, 602–607 **(2011)**

70. Dhineshbabu N.R., Rajendran V., Nithyavathy N. and Vetumperumal R., Study of structural and optical properties of cupric oxide nanoparticles, *Appl. Nanosci.*, **6**, 933–939 **(2016)**

71. Rehman S., Mumtaz A. and Hasanain S.K., Size effects on the magnetic and optical properties of CuO nanoparticles, *J. Nanoparticle Res.*, **13**, 2497–2507 **(2011)**

72. Chatzimitakos T.G. and Stalikas C.D., Qualitative Alterations of Bacterial Metabolome after Exposure to Metal Nanoparticles with Bactericidal Properties: A Comprehensive Workflow Based on 1 H NMR, UHPLC-HRMS and Metabolic Databases, *J. Proteome Res*., **16**, 3322–3330 **(2016)**

73. Konar S., Kalita H., Puvvada N., Tantubay S., Mahto M.K., Biswas S. and Pathak A., Shape-dependent catalytic activity of CuO nanostructures, *J. Catal.*, **336**, 11–22 **(2016)**

74. Huang J., Fu G., Shi C., Wang X., Zhai M. and Gu C., Novel porous CuO microrods: synthesis, characterization and their photocatalysis property, *J. Phys. Chem. Solids*, **75**, 1011–1016 **(2014)**

75. Hemalatha S., Photocatalytic Degradation of Vat Red 13 by Green Synthesized Copper Oxide Nanocatalyst, *Int. J. Chem. Sci.*, **16**, 1–8 **(2018)**

76. Aminuzzaman M., Kei L.M. and Liang W.H., Green Synthesis of Copper Oxide (CuO) Nanoparticles using Banana Peel Extract and Their Photocatalytic Activities, AIP Conference Proceedings, 1828 020016 **(2017)**

77. Mahmood Aliofkhazraei, Handbook of Nanoparticles, Springer International Publishing, Cham **(2015)**

78. Whittingham E.M.S., Jacobson A.J. and Barrer R.M., Intercalation Chemistry Hydrothermal Chemistry of Zeolites Size and Shape Characterization of Fibrous Zeolites by Electron Microscopy, *Intercalation Chem.*, **3**, 1982–1983 **(1983)**

79. Hamedi M., Wigenius J., Tai F., Björk P. and Aili D., Linköping University Post Print Polypeptide-guided assembly of conducting polymer nanocomposites Polypeptide-Guided Assembly of Conducting Polymer Nanocomposites, *Nanoscale*, **8**, 2058–2061 **(2010)**

80. Lin Q., Li Y. and Yang M., Tin oxide/graphene composite fabricated via a hydrothermal method for gas sensors working at room temperature, *Sensors Actuators B Chem.*, **173**, 139–147 **(2012)**

81. Aliofkhazraei M., Handbook of Nanoparticles, Springer International Publishing, Cham **(2016)**

82. Mageshwari K., Sathyamoorthy R. and Park J., Photocatalytic activity of hierarchical CuO microspheres synthesized by facile reflux condensation method, *Powder Technol.*, **278**, 150–156 **(2015)**

83. Suslick K.S., Applications of Ultrasound to Materials Chemistry, *MRS Bull.*, **20**, 29–34 **(1995)**

84. Gutlich P., Editorial board page for Comments on Inorganic Chemistry, Comments Inorg. Chem. Frontiers **(1981)**

85. Djurišić A.B., Leung Y.H. and Ching Ng A.M., Strategies for improving the efficiency of semiconductor metal oxide photocatalysis, *Mater. Horizons*, **1**, 400 **(2014)**

86. Hisatomi T., Kubota J. and Domen K., Recent advances in semiconductors for photocatalytic and photoelectrochemical water splitting, *Chem. Soc. Rev*., **43**, 7520–7535 **(2014)**

87. Riga A., Soutsas K., Ntampegliotis K., Karayannis V. and Papapolymerou G., Effect of system parameters and of inorganic salts on the decolorization and degradation of Procion H-exl dyes. Comparison of H2O2/UV, Fenton, UV/Fenton, TiO_2/UV and TiO_2/UV/H_2O_2 processes, *Desalination*, **211**, 72–86 **(2007)**

88. Chiou C.,Wu C. and Juang R., Influence of operating parameters on photocatalytic degradation of phenol in UV/TiO_2 process, *Chem. Eng. J.*, **139** 322–329 **(2008)**

89. Cui Y., Ding Z., Liu P., Antonietti M., Fu X. and Wang X., Metal-free activation of H2O2 by g-C 3N4 under visible light irradiation for the degradation of organic pollutants, *Phys. Chem. Chem. Phys.*, **14**, 1455–1462 **(2012)**

90. Kamat P.V., Manipulation of Charge Transfer Across Semiconductor Interface, *J. Phys. Chem. Lett.*, **3**, 663–672 **(2012)**

91. Szczepankiewicz S.H., Colussi A.J. and Hoffmann M.R., Infrared spectra of photoinduced species on hydroxylated titania surfaces, *J. Phys. Chem. B.*, **104**, 9842–9850 **(2000)**

92. Henderson M.A., A surface science perspective on TiO_2 photocatalysis, *Surf. Sci. Rep.*, **66**, 185–297 **(2011)**

93. Wu S. and Guo J., The study of sensors market trends analysis based on social media, *Sensors and Transducers*, **159**, 374–378 **(2013)**

94. Hansen B.J., Kouklin N., Lu G., Lin I.K., Chen J. and Zhang X., Transport, analyte detection and opto-electronic response of p-type CuO nanowires, *J. Phys. Chem. C.*, **114**, 2440–2447 **(2010)**

95. Mahmoodi N.M., Arami M., Limaee N.Y. and Tabrizi N.S., Kinetics of heterogeneous photocatalytic degradation of reactive dyes in an immobilized TiO2 photocatalytic reactor, *J. Colloid Interface Sci*., **295**, 159–164 **(2006)**

96. Li J., Sun F., Gu K., Wu T., Zhai W., Li W. and Huang S., Preparation of spindly CuO micro-particles for photodegradation of dye pollutants under a halogen tungsten lamp, *Appl. Catal. A Gen.*, **406**, 51–58 **(2011)**

97. Daneshvar N., Salari D. and Khataee A.R., Photocatalytic degradation of azo dye acid red 14 in water on ZnO as an alternative catalyst to TiO_2, *J. Photochem. Photobiol. A Chem*., **162,** 317–322 **(2004)**

98. Lei P., Chen C., Yang J., Ma W., Zhao J. and Zang L., Degradation of dye pollutants by immobilized polyoxometalate with H_2O_2 under visible-light irradiation, *Environ. Sci. Technol.*, **39**, 8466–8474 **(2005)**

99. Zhang J., Shao C., Li X., Xin J., Tao R. and Liu Y., Assembling n-Bi2MoO6 Nanosheets on Electrospun p-CuAl2O4 Hollow Nanofibers: Enhanced Photocatalytic Activity Based on Highly

Efficient Charge Separation and Transfer, *ACS Sustainable Chemistry & Engg.*, **6**, 10714-10723 **(2018)**

100. Takahara Y.K., Hanada Y., Ohno T., Ushiroda S., Ikeda S. and Matsumura M., Photooxidation of organic compounds in a solution containing hydrogen peroxide and TiO_2 particles under visible light, *J. Appl. Electrochem.*, **35**, 793–797 **(2005)**

101. Stark Y.J., Bend N. and Data P.P., C. Interaction, (12) United States Patent, 2 **(2012)**

102. Khataee A.R. and Kasiri M.B., Photocatalytic degradation of organic dyes in the presence of nanostructured titanium dioxide: Influence of the chemical structure of dyes, *J. Mol. Catal. A Chem.*, **328**, 8–26 **(2010)**

103. Kumar P.S., Lakshmi Prabavathi S., Indurani P., Karuthapandian S. and Muthuraj V., Light assisted synthesis of hierarchically structured Cu/CdS nanorods with superior photocatalytic activity, stability and photocatalytic mechanism, *Sep. Purif. Technol.*, **172**, 192–201 **(2017)**

104. Borchert H., Shevchenko E.V., Robert A., Mekis I., Kornowski A., Grübel G. and Weller H., Determination of nanocrystal sizes: A comparison of TEM, SAXS and XRD studies of highly monodisperse CoPt 3 particles, *Langmuir.*, **21**, 211931–1936 **(2005)**

105. El-Bahy Z.M., Ismail A.A. and Mohamed R.M., Enhancement of titania by doping rare earth for photodegradation of organic dye (Direct Blue), *J. Hazard Mater.*, **166**, 138–143 **(2009)**

106. Chakraborty A., Islam D.A. and Acharya H., Facile synthesis of CuO nanoparticles deposited zeolitic imidazolate frameworks (ZIF-8) for efficient photocatalytic dye degradation, *J. Solid State Chem.*, **269**, 566–574 **(2019)**.

(Received 18th June 2020, Accepted 27th August 2020)